SUPERSONIC COMBUSTION RAMJET PROPULSION EXPERIMENTS IN A SHOCK TUNNEL

A. Paull, R.J. Stalker and D.J. Mee

Department of Mechanical Engineering

The University of Queensland

Brisbane, 4072 Queensland Australia

ABSTRACT

Measurements have been made of the propulsive effect of supersonic combustion ramjets incorporated into a simple axisymmetric model in a free piston shock tunnel. The nominal Mach number was 6, and the stagnation enthalpy varied from 2.8 MJ kg^{-1} to 8.5 MJ kg^{-1}. A mixture of 13% silane and 87% hydrogen was used as fuel, and experiments were conducted at equivalence ratios up to approximately 0.8. The measurements involved the axial force on the model, and were made using a stress wave force balance, which is a recently developed technique for measuring forces in shock tunnels. A net thrust was experienced up to a stagnation enthalpy of 3.7 MJ kg^{-1}, but as the stagnation enthalpy increased, an increasing net drag was recorded. Pitot and static pressure measurements showed that the combustion was supersonic.

The results were found to compare satisfactorily with predictions based on established theoretical models, used with some simplifying approximations. The rapid reduction of net thrust with increasing stagnation enthalpy was seen to arise from increasing precombustion temperature, showing the need to control this variable if thrust

performance was to be maintained over a range of stagnation enthalpies. Both the inviscid and viscous drag were seen to be relatively insensitive to stagnation enthalpy, with the combustion chambers making a particularly significant contribution to drag. The maximum fuel specific impulse achieved in the experiments was only 175 sec., but the theory indicates that there is considerable scope for improvement on this through aerodynamic design.

1. INTRODUCTION

The supersonic combustion ramjet, or "scramjet", has existed as a concept for some decades (e.g. Ferri 1964, Swithenbank 1967, Jones and Huber 1978, Billig 1993). Essentially, it generates a propulsive effect through heat addition, by combustion, at supersonic speeds. In principle, it is able to operate at any flight speed, but a practical limit seems to exist at 4 or 5 km s^{-1}. To explore the potential of the scramjet, the ability to conduct routine experimentation at such speeds is essential.

For speeds in excess of 2 km s^{-1}, power and materials limitations have forced ground facilities to adopt the principle of impulse operation, with test times of only a few milliseconds. The most successful facility of this type has proven to be the shock tunnel, and indeed, substantial scramjet experimentation has been done in shock tunnels (e.g. Stalker and Morgan 1984).

However, the scramjet is a propulsive device, and the ultimate test of a propulsive device is its ability to generate thrust when installed in a flight vehicle. Therefore experimentation in which thrust or drag is measured on vehicle models in a shock tunnel

can be expected to be an important part of scramjet research.,

Methods of measuring forces on a shock tunnel model have been reported by previous investigators (Bernstein 1982, Jessen and Grönig, 1989, Naumann et al 1993), but these are only effective with test models which are relatively small with respect to the tunnel size. For a scramjet model to produce thrust, vigorous combustion in the combustion chambers is required and, with the combinations of pressure and Mach number which can be achieved in a shock tunnel, a not insubstantial length is required for the combustion chambers. Since the combustion chambers must be integrated into a complete model it is, therefore, very difficult to retain a model size which is small in relation to the tunnel size.

This paper reports measurements of the effect of stagnation enthalpy on the thrust and drag of a quasi-axisymmetric scramjet model. It is of particular relevance to the possible use of scramjets to propel acceleration vehicles, where one of the effects of the continually changing flight velocity will be a changing stagnation enthalpy. The model incorporated intakes, combustion chambers and thrust nozzles, and was therefore aerodynamically complete. Having regard to the difficulty noted in the previous paragraph, the measurements were accomplished by employing a stress wave force balance (Sanderson and Simmons 1991), which will be explained in more detail below, and which does not require a model which is small in relation to the tunnel size. A positive resultant thrust was measured - i.e. the total thrust generated was greater than the drag of the complete configuration - though only over a limited range of test section velocities.

The measurements are also compared with theoretical predictions. Though intakes, combustion chambers and thrust nozzles have all been the subject of research separately, an experimental study involving all three elements combined into an integrated configuration has not been reported, at least, in the open literature. Therefore the comparison between theory and experiment is of considerable interest. The model was designed to facilitate this comparison, and so an outstanding propulsive performance was neither expected nor achieved.

The shock tunnel in which the experiments were conducted is briefly described first, paying attention to limits on the test time and the test section flow produced. Then the main features of the model are described, followed by a short discussion of the principle of the stress wave force balance. The application of the balance to this problem is outlined, and some typical data recordings are presented. Following this, theoretical predictions of the effect of stagnation enthalpy on the thrust are developed. These predictions are then compared with measurements of the thrust, the comparison being assisted by some pressure measurements in one of the combustion ducts of the model.

2. THE SHOCK TUNNEL

The experiments were done in the free piston shock tunnel T4 at The University of Queensland, as shown in fig. 1. This consisted of a compression tube, 27 m long and 228 mm in diameter, in which the temperature and pressure of the driver gas was raised by a free piston compression process immediately prior to diaphragm rupture. The shock tube was 10 m long and 76 mm in diameter, and for these tests, supplied test gas to a contoured hypersonic nozzle which expanded from a throat diameter of 25 mm to a

diameter of 263 mm at the test section.

The nozzle stagnation pressure was monitored during each test by a PCB quartz piezoelectric pressure transducer located 60 mm upstream of the downstream end of the shock tube, and a typical record is shown in fig. 2(a). It can be seen that after the initial peak at shock reflection, the pressure remained constant within 20% for approximately 2 millisec. A mixture of Argon with Helium was used as the driver gas, and the ratio of the two was varied as the stagnation enthalpy was varied to ensure that a similar period of approximately constant nozzle stagnation pressure was maintained throughout the tests.

Measurements with a time-of-flight mass spectrometer on the nozzle axis were used to determine when the test section become contaminated by driver gas, and results are shown in fig. 2(b)*. It can be seen that, although the time to contamination exhibits substantial shot to shot variation at a given stagnation enthalpy, a period of 1 millisecond or more of flow with a contamination level of less than 10% exists up to stagnation enthalpies of 10 MJ kg^{-1}. This is in excess of the stagnation enthalpies used in the experiments.

The test section conditions were calculated using a non-equilibrium nozzle code (Lordi et al 1966) for a steady expansion in a hypersonic nozzle from known reservoir conditions to a given Pitot pressure level. The reservoir conditions were determined by first obtaining the pressure and stagnation enthalpy after shock reflection from measurements of the shock speed and shock tube filling pressure. It is then assumed that an isentropic

*The authors would like to thank K. Skinner for the use of this data.

expansion to the measured nozzle reservoir pressure occurs. This pressure varied from 34 MPa to 40 MPa, with an underlying trend to increase with increasing stagnation enthalpy superimposed on a random shot to shot variation. This is reflected in the Pitot pressure measurements shown in fig. 3(a). The ratio of Pitot pressure to nozzle reservoir pressure was $(14.1 \pm 0.6) \times 10^{-3}$, and showed no variation with stagnation enthalpy so the scatter in Pitot pressure is due largely to variation in nozzle reservoir pressure. Using the value of 14.1×10^{-3} for the nozzle calculations, the test section conditions shown in fig. 3(b) were obtained.

The test section flow was calibrated for uniformity and flow divergence by traversing with a Pitot rake. A typical result is shown in fig. 4.**. Two traverses, taken at 100 mm and 300 mm from the nozzle exit respectively, are shown in the upper half of the figure. The position of the model is shown in the lower half. The cone of uniform flow starts well upstream of the model, and the traverses show that a reasonably uniform test core, without observable flow divergence, persists to a distance well downstream of the model. The location of a Pitot probe, which was used to monitor the Pitot pressure during tests on the model, is also shown in the bottom half of the figure and yielded the results of fig 3(a).

3. THE MODEL

The scramjet model is shown in fig. 5 with half of the cowl removed. It consists of an axisymmetric centrebody, with six combustion chambers and associated intakes symmetrically arranged about its periphery, and separated from each other by six

**The authors would like to thank S. Overton for the use of this data.

splitters. The centrebody has a conical forebody with an 9° half angle, and a conical afterbody of 10° half angle. The combustion chamber intakes consist of compression ramps formed by the splitters which deflect the flow in the shock layer on the conical forebody through an angle of 8° parallel to its surface, with the leading edge of the cowl swept at an angle chosen to trap the nearly two-dimensional shocks so formed, and prevent them spilling into the freestream. The internal surface of the cowl is parallel to the forebody surface, and the external chamfer on the cowl leading edges makes an included angle of 8.5° in the freestream direction. The leading edge of the compression ramps is 10 mm wide, measured in the radial direction.

After the flow in the forebody shock layer has passed through the shock formed by one of the compression ramps, and its reflection, it is then turned to become parallel to the freestream, and enters one of the combustion chambers. These are 59 mm long, and each has a cross-section which is an arc of an annulus of major diameter 67 mm and minor diameter 51 mm, subtending an angle of 23° at the centreline. The fuel injection orifices were located at the beginning of the cylindrical part of the centrebody, and were therefore at the upstream end of the combustion chambers. There was one orifice to each combustion chamber. They were 2 mm in diameter, angled at 30° to the centreline, and injected in the downstream direction.

At the downstream end of the combustion chambers, the sidewalls deflect through an angle of 12°, and the conical afterbody begins, to make an array of thrust generating surfaces. These are terminated when the 12° surfaces meet, and when the afterbody diameter becomes 25 mm, at which point the centrebody becomes cylindrical again. The

trailing edge of the cowl also makes an internal angle of 7° with the freestream direction, and this is expected to add a small increment of thrust.

The model as it is mounted in the test section is shown in fig. 6 . The model is attached via the valve system to the fuel tank, which is itself attached to the stress wave bar of the stress wave balance. The stress wave bar is suspended from ports in the tunnel dump tank by two fine wires. The valve assembly, the fuel tank and the stress wave bar are surrounded by an aerodynamic shroud, and the only contact of the model assembly with the shroud is through a flexible "O" ring seal on the parallel section downstream of the conical afterbody of the model. A streamwise section of the model assembly is shown in fig. 6 . It can be seen that a 10 mm hole is drilled along the model axis to carry the fuel, which is distributed to the injectors as shown.

A schematic depicting the operation of the valve is shown in fig. 6 . The solenoid valve, S, is normally closed, and the fuel tank is filled before a test. The cavity G is maintained at the fuel pressure, so the fuel valve F is closed. When the tunnel is fired, its recoil closes a switch which activates the solenoid valve, causing it to open, and allow the fuel to flow out of cavity G to vacuum. The pressure in cavity G falls, the fuel valve F opens, and fuel flows through it to the fuel pipe. As it does so, its pressure is monitored by a PCB type 111A quartz piezoelectric pressure transducer. When the pulse of test gas has passed, the solenoid valve closes again, the fuel continues to flow into cavity G through the bleed orifice O, the pressure in the cavity builds up, and valve F closes.

The centrebody and splitters of the model are made of aluminium alloy, while the cowl

was made of stainless steel. The fuel tank and valve assembly is made of stainless steel.

4. THE STRESS WAVE FORCE BALANCE

It will be observed that the length of the model is not small with respect to the tunnel size. Also it is noted by Sanderson & Simmons (1991) that stress waves, induced in the model by the flow starting process, propagate along the model with speeds of the order of 3000 to 5000 m s^{-1}, which is of the same magnitude as the flow speed. Therefore, the many stress wave reflections which must occur before the model can be said to behave as a rigid one will correspond to a large number of flow passes over the model, requiring a time which normally exceeds the test time.

Fortunately, the stress waves which are the source of this difficulty can themselves be exploited to measure the force on the model. If strain gauges are placed on the model support sting adjacent to the base of the model, and the time history of stress waves passing into the sting is recorded, this recording can be deconvoluted to yield the force on the model. The simplest case of deconvolution occurs when the model is simply an extension of the stress bar and the force is applied as a step change in time at its upstream end, in which case the strain gauges record the passage of a stress wave which directly represents the applied load. This, in fact, is identical to the bar gauge which is used for measuring transient pressures. However as the models become more complicated, so does the deconvolution.

When Sanderson and Simmons first proposed this technique, they applied it to measurement of drag on a short cone. In that case the internal stress wave effects were

unimportant, but subsequent measurements on a 425 mm long cone, (Tuttle, 1990) where they were important, showed that they could be taken into account satisfactorily. Measurements on a long blunt cone (Porter, 1993) then showed that non-uniformity in the axial load distribution was no impediment to use of the method.

Now, for the purposes of stress wave analysis, the relatively slender models which are of interest here may be treated as one-dimensional, with cross-sectional area varying in the axial direction. Strictly, each axial element of the model produces a particular signal at the strain gauges, which therefore give an output which depends on the force distribution on the model, as well as the total force. Fortunately, numerical analysis (Simmons et al 1993), and the experiments noted in the previous paragraph, indicate that for these conical models and the times of interest here, the distribution of force is unimportant. When this is so, the relation between the output of the strain gauges, y(t), and the force applied to the model, u(t), may be written as

$$y(t) = \int_0^t g(t-\tau)\, u(\tau)\, d\tau ,$$

where g(t) is an impulse response function which relates y(t) and u(t). With g(t) determined, either numerically or by calibration, this expression allows numerical deconvolution procedures to be applied to y(t) to yield u(t).

The model employed here was larger and more complicated than the cones of the previous studies, so it was necessary to again check the distribution of force was not important. This was done numerically. A two-dimensional axisymmetric finite element 70 x 6 mesh was made to represent the model and fuel tank, and three loading

distributions were applied independently to approximately represent the loading on the model during a test. One represented the drag of the model, and was applied as a load distributed over the surface of the model. One represented the thrust due to injection of the fuel, and was applied as a point load at the location of the injection orifices. The third one represented the thrust due to mixing and combustion, and was applied as a distributed load on the thrust surface. The variation with time of each of these is shown in fig. 7(a). Together these three inputs produced a simulated strain gauge response. This was then deconvolved, using an impulse response function g(t) which was determined for a single point load applied at the nose, to see if the applied time history of the force on the model could be recovered. The result is shown as the solid line in fig. 7(b), where it is compared with the sum of the three forces acting on the model. It can be seen that the deconvolved signal is in good agreement with the input signal, signifying that the measured force was indeed independent of its distribution.

Having thus established that no significant error was involved in taking the force as applied at the nose, the impulse response function for such a force was determined experimentally. This was done by vertically suspending the model and fuel tank, attached to the stress bar, by a fine wire attached to the nose. The wire was cut close to the nose tip to effect a sudden removal of the tensile load, thereby producing the equivalent of a step increase in drag. The resulting strain gauge output shown in fig. 8(a), gave the step response for the system, and the impulse response was found by differentiating this with respect to time. This approach had the benefit that any effects of stress wave damping, though small, would be captured in the impulse response function. With a suitable g(t) thus defined in eqn (1), the deconvolution could then proceed numerically, by the time-

domain iterative method of Prost & Goutte (1984), to yield the axial force. This process yielded a random error of $\pm 10\%$ in the axial force, but no detectable systematic error.

5. FORCE MEASUREMENTS

A strain gauge output obtained during a test is shown in fig. 8(b). Fuel injection is timed so that a nearly constant fuel mass flow is maintained during the test time, and this has the consequence that the thrust due to fuel injection grows before the test time begins. This is evident in the lower frequency oscillation in the strain gauge output, before the initiation of test flow. As the test flow begins, the frequency increases.

Using the impulse response function derived from fig. 8(a), the output of the strain gauge in fig 8(b) is deconvolved numerical to yield axial force records, as shown in fig. 9(b). There are some spurious low amplitude oscillations on these records, which are ascribed partly to non-axial vibrations transmitted to the stress wave bar from the surroundings, and partly to imperfections in the deconvolution process, but these have only a small effect on the accuracy of the records. The test section Pitot pressure, as well as the fuel supply pressure for the fuel-on cases, are shown in fig. 9(a), and both are seen to be nearly constant during the test time.

It can be seen in fig. 9(b) that, for the fuel-off case, a drag of approximately 150 N is experienced by the model during the test time. When fuel is injected with nitrogen as the test gas, the drag is reduced and, before the test flow arrives, a thrust due to the reaction of the fuel jets is evident. This thrust increment appears to increase when the flow arrives but this is a spurious effect, due to the change in drag associated with the change

in test gas. When fuel is injected with air as the test gas, the axial force variation follows that of fuel injected into nitrogen, until the fuel ignites in the combustion chambers, when the axial force increases in the thrust direction, reaching a plateau at approximately 50 N of thrust.

Measurements of the axial force with and without fuel injection were taken for a range of stagnation enthalpies. However, before considering the results of these measurements, a theoretical treatment of the effects giving rise to this force is required, and this will be done after an analysis of the mode of metering the fuel injection.

6. FUEL INJECTION

Initially, it was intended that hydrogen be used as the fuel, as previous experiments (Stalker & Morgan, 1984) had suggested that at a combustion chamber length of 60 mm, and the pressures of approximately 1 atm, which it was thought would be achieved, would be adequate for combustion. However, hydrogen did not burn, due probably to the occurrence of expansion waves in the combustor, and a mode of fuel injection which was different to the original experiments. Therefore silane was added to the hydrogen to promote combustion.

A system for mixing silane and hydrogen was available, but required excessive time to produce a uniform mixture. Therefore the concentration of silane was monitored for each test by using the pressure transducer in the fuel supply duct and the pressure in the fuel tank, measured before and after a test, together with the following analysis.

Assuming the flow through the fuel injection orifices is sonic, the fuel mass flow rate at any instant may be written as

$$\dot{m}_F = \{F(\gamma) A_c / R_0 T\} \sqrt{M}\, P_F = B \sqrt{M}\, P_F$$

where $B = F(\gamma)\, A_c/R_0T$, $F(\gamma)$ is a function of the ratio of specific heats, A_c is the effective area of the orifices, R_0 is the universal gas constant, T is the temperature in the fuel injection system, which is taken as being constant, M is the molecular weight of the fuel, and P_F is the pressure measured in the fuel supply duct. From this, the mass Δm leaving the fuel tank in time t is

$$\Delta m = B \sqrt{M} \int_0^t P_F\, dt \quad .$$

Using the change in pressure in the fuel tank, ΔP_r, Δm may also be written as

$$\Delta m = M . \Delta P_r \; V/R_o T \quad ,$$

where V is the volume of the fuel tank. Equating the expressions for Δm leads to

$$M = \left\{ B (R_0 T/V) \int_0^t P_F\, dt / \Delta P_r \right\}^2 \quad .$$

The fuel supply valve opened in approximately 6 millisec, and closed approximately 100 millisec later. By monitoring P_F during this time, the value of the integral in the above equation could be obtained, and ΔP_r could be measured by observing the pressure in the fuel tank before and after a test. A previous calibration for B, obtained by operating the fuel system with various known amounts of silane in the gas mixture, then allowed M to be determined, and hence the silane concentration as well as the mass flow through the fuel orifices is also known. This was finally corrected for adiabatic expansion in the fuel tank by multiplying the mass flow by 1.08. The equivalence ratio was then calculated as the ratio of this mass flow to the mass flow of fuel required to consume all the oxygen in the air passing through the duct.

7. ANALYSIS OF PROPULSIVE PERFORMANCE

The installed propulsive performance of engines in an aerodynamic vehicle is commonly assessed in terms of the thrust generated versus the drag to be overcome. When the function of the engine is largely independent of the vehicle aerodynamics, it is possible to adopt a simple view, taking thrust as an engine property, and drag as a property of the vehicle. However, for scramjets, which are integrated into the flow field about the body, such an approach is not possible. In this case it is more suitable to relate the performance to fuel injection, estimating the change in axial force on the configuration produced by injecting the fuel.

Therefore the analysis proceeds by first considering the drag in the absence of fuel injection, before going on to treat the effect of the combustion of the fuel. It should be noted that, not withstanding the attempt to use a simple model configuration, the details of the flow are so complicated that a rigorous analysis would be extremely difficult. Thus, some simplifying approximations are made but, as will be seen below, the analysis which results adequately predicts the experimental results.

8. INVISCID FUEL-OFF DRAG

Intake Assembly. The flow over the conical forebody and the intakes is shown schematically in fig. 10. The conical shock originating at the tip of the cone causes a uniform pressure over the region a of the cone surface. The splitters are machined so that the inlet ramp surface is always normal to the cone surface, as shown in section AA. It is assumed that this leads to shocks which are also normal to the cone surface, and that the pressure in the regions b is uniform and is given by the pressure downstream of a

two-dimensional oblique shock formed by the leading edge of the inlet ramp. The effect of shock-boundary layer interactions is ignored, since they do not affect the overall pressure rise, and the dispersion of the pressure rise at the foot of the shock which they do cause is likely to raise the force on the surface upstream of the shock by as much as it reduces it downstream. As shown in section AA, the outer surface area of the inlet duct is greater than the inner area, and this effect is taken into account.

Calculations indicate that the conical shock from the tip of the cone should pass inside the cowl, as shown in figure 10(a). Further calculations showed that if it passed outside of the cowl, the leading edge bevel would induce shock detachment. Detachment was not evident in luminosity photographs of the flow, and so the drag could be estimated by taking the free stream to be directly incident on the exterior surfaces of the cowl. The pressure on the bevel was obtained by treating it as part of an infinite, swept, leading edge.

The maximum temperature in the inlet was less than 2200 K, implying that no dissociation took place. Thus the flow model outlined was used, with a ratio of specific heats of 1.4. The inviscid drag of the intake assembly, comprising the conical forebody, the inlets and the cowl exterior, expressed in Newtons, was calculated to be

$$25 \times 10^{-5} P_P$$

with the Pitot pressure P_P in units of N m^{-2}. This was independent of the expected variation in the freestream Mach number. The major contributions were the drag on the inlet ramps, or splitters, at 50%, the drag on the forecone, at 20%, and the drag on the cowl leading edge bevel, at 25%.

Combustion Chambers. The inviscid drag of the combustion chambers is zero, since their cross-sectional area is constant. However, the pressure and Mach number in the combustion chambers is required in order to calculate the level of thrust produced in the expansion nozzle. These may be obtained from the relations for adiabatic flow in a streamtube (e.g. Hall 1951) which can be written as

$$\frac{A_f}{A_\infty} \exp(-\Delta S/R) = \frac{M_\infty}{M_f}\left(\frac{1+\frac{\gamma-1}{2}M_f^2}{1+\frac{\gamma-1}{2}M_\infty^2}\right)^{(\gamma+1)/2(\gamma-1)},$$

and

$$\frac{P_f}{P_\infty} = \frac{A_\infty}{A_f}\frac{M_\infty}{M_f}\left(\frac{1+\frac{\gamma-1}{2}M_\infty^2}{1+\frac{\gamma-1}{2}M_f^2}\right)^{1/2},$$

where A_∞ is the cross-sectional area in the freestream of the streamtube captured by the intake, M_∞ and P_∞ are the freestream Mach number and pressure, A_f is the total cross-sectional area of the combustion chambers, and M_f and P_f are the Mach number and pressure there. Since the conical shock from the cone passes inside the cowl leading edges, no "spilling" of the flow from the intake takes place, and A_∞ can be taken as the area defined by the projection of the cowl leading edges onto a plane normal to the flow direction. The entropy rise per unit mass of gas associated with the three shocks through which the flow is compressed is ΔS, and R is the gas constant per unit mass. When these relations are combined with the dimensions of the model, it is found that, with $\gamma = 1.4$, $M_f = 4.0$ at $M_\infty = 6.1$ and increases by 10% for each 10% increase in M_∞. P_f may be written as

$$P_f = (0.56 - 0.059\,M_\infty)P_p \qquad (1)$$

which is a form convenient for later use. Estimates indicate that the effect of the displacement thickness of the boundary layer on the combustion chamber cross-section is

small enough to be ignored.

Predicted values of P_f are compared with measurements in fig. 15. The measurements are corrupted by the persistence of waves in the flow, due to intake-combustion chamber mismatch, but it can be seen that the predictions are not inconsistent with the mean level.

Expansion Nozzles. The surfaces of the expansion nozzles are formed by the conical afterbody and adjacent splitters, and the pressures experienced on these surfaces determine all but a few per cent of the thrust acting on the model. To calculate these pressures, it is assumed that the transverse curvature of the conical afterbody may be neglected, and the flow field at the corner between the afterbody and the splitters is that produced by double expansion of a streamwise corner, as shown in fig. 11.

The trace of the wave pattern in two cross flow planes, X and Y, is shown in the figure, demonstrating the conical nature of the flow. Taking the plane X, region f corresponds to uniform flow which is outside of the zone of influence of the two surfaces. Outside the zone of influence of the streamwise corner, the flow passes through one of two centred Prandtl-Meyer expansions to produce the two uniform flow regions f_1 and f_2. For the part of the flow field which is within the zone of influence of the streamwise corner, an analytic solution is not known, but numerical solutions (Anderson and Nangia 1977) indicate that each of the flow regions f_1 and f_2 passes through one of two further Prandtl-Meyer expansions to produce another region of uniform flow f_{12}. The total deflection angle experienced in passing from f to f_{12} is the same, irrespective of whether the passage is accomplished through f_1 or f_2. Since the properties of the flow produced by a Prandtl-

Meyer expansion are uniquely related to the deflection angle, the properties in f_{12} are uniquely determined. Thus the flow over each of the two adjacent surfaces can be analysed as a uniform flow, produced by the deflection of the surface itself, with the deflection of the adjacent surface producing a simple Prandtl-Meyer expansion of that uniform flow.

This model was used to obtain the pressure distribution on the conical afterbody and adjacent splitter surfaces, taking account of the expansion wave from the cowl trailing edge, and reflection from the plane of symmetry between two splitters, in the same way. A simple graphical procedure allowed the pressure distribution to be established with sufficient accuracy. The thrust was then obtained by integration of this pressure distribution, taking account of the reduction of area with downstream distance of the conical afterbody. The calculations were performed for a perfect gas with a ratio of specific heats of 1.4.

Results are presented in fig. 12 for a range of combustion chamber Mach numbers. For comparison, the thrust which would be obtained with one-dimensional flow through a nozzle of the same area ratio also is shown, and it is seen that the difference between the two increases with Mach number, the thrust of the three-dimensional nozzle falling as the one-dimensional one increases. Clearly, the three-dimensional flow makes better use of the thrust surfaces at lower Mach numbers than at the higher ones.

9. VISCOUS FUEL-OFF DRAG

To assess the viscous drag of a surface, it is first necessary to determine whether the

boundary layer is laminar or turbulent. Previous experiments (He and Morgan 1994) have shown that transition occurs on a flat plate in the shock tunnel at a Reynolds' number, based on distance from the leading edge, of approximately 2 x 10^6. Applying this to the model used in the experiments, the boundary layer flow on the inlet splitter face, the internal inlet, surfaces of the cowl, and the exterior surface of the cowl, along its full length, is expected to be laminar. The Reynolds' number on the conical forebody may reach 4 x 10^6 but, allowing for the higher transition Reynolds' numbers on a cone, this too is expected to exhibit predominantly laminar flow.

Thus for these surfaces, the local skin friction coefficient is given by (e.g. Hayes and Probstein 1959)

$$\begin{aligned} c_f &= 2\tau_w/\rho_e u_e^2 \\ &= 0.664\, n\left(\rho^* u^* / \rho_e \mu_e\right)^{0.5} / R_{ex}^{0.5} \end{aligned}$$

where ρ_e, u_e and μ_e are the density, velocity and coefficient of viscosity in the external stream adjacent to the boundary layer, τ_w is the skin friction per unit area, R_{ex} is the Reynold's number based on the external stream properties and the distance from the leading edge, n = 1 and $\sqrt{3}$ for a flat plate and a cone respectively, and ρ^* and μ^* are the density and viscosity at a reference temperature T^*, given by

$$T^*/T_e = 0.5\left(1 + T_w/T_e\right) + 0.0384\, M_e^2$$

where T_e and T_w are temperature in the external stream and at the wall respectively, and M_e is the external stream Mach number. Due to the reduction in Reynolds's number as the stagnation enthalpy increases, the skin friction increases with stagnation enthalpy, H_s, and the total drag, in Newtons, for the surfaces noted in the paragraph above is

$$(3.09 + 0.55\, H_s) \times 10^5\, P_t$$

where H_s is in MJ/kg. Of this the forecone, the inlet splitter faces, the interior inlet surface of the cowl, and the exterior surface of the cowl all contributed approximately equal portions.

The Reynolds' number of the flow in the combustion chambers is such that, taking account of the shock-boundary interactions in the inlets, the boundary layer flow is expected to be turbulent. A review of turbulent skin friction by Hopkins and Inouye (1971) indicates that the theory of Spalding and Chi is most suited to the low values of T_w/T_e experienced here. This theory obtains the skin friction in compressible flow from incompressible values by using the transformations

$$\bar{c}_f = F_c\, c_f ,$$
$$\text{and } \bar{R}_{ex} = F_x\, R_{ex} ,$$

where the bar denotes the incompressible values. F_c and F_x are given here by

$$F_c = 0.18\, M_e^2 \left(\sin^{-1}\alpha + \sin^{-1}\beta\right)^{-2} ,$$
$$\text{and } F_x = \left(\sin^{-1}\alpha + \sin^{-1}\beta\right)^2 \left\{0.18\, M_e^2 \left(T_w/T_e\right)^{0.702} \left(T_w/T_{aw}\right)^{0.772}\right\}^{-1}$$
$$\text{where } \alpha = \left(2A^2 - B\right)\left(4A^2 + B^2\right)^{-0.5} ,$$
$$\text{and } \beta = B\left(4A^2 + B^2\right)^{-0.5} ,$$
$$\text{with } A^2 = 0.18\, M_e^2\, T_e/T_w ,$$
$$\text{and } B = \left(1 + 0.18\, M_e^2 - T_w/T_e\right) T_e/T_w .$$

T_{aw} is the stagnation temperature in the external stream. The incompressible values of skin friction were taken from the relation

$$\bar{c}_f = 0.060\, \bar{R}_{ex}^{-0.2} .$$

The effective origin of the turbulent boundary layer was obtained by estimating the laminar boundary layer thickness at the entrance to the combustion chambers after

compression to the combustion chamber pressure, using this to indicate the effective origin of a laminar boundary layer, and assuming that the turbulent boundary layer originated at half that distance upstream. Using this theory, the skin friction drag in the combustion chambers, expressed in Newtons, was calculated to be

$$(35.1 + 0.82\ H_c) \times 10^{-5}\ P_f$$

where P_f is in units of N m^{-2}. There is negligible variation over the range of Mach numbers experienced without fuel injection.

The boundary layer flow in the expansion nozzles was also taken to be turbulent, as the favourable pressure associated with the expansion corner was estimated as insufficient to cause relaminarisation (Narasimha and Viswanath 1975). Noting that the skin friction coefficient varies slowly with Reynold's number it is assumed to be unchanged across the expansions and therefore, by also assuming that the velocity is unchanged, the skin friction at any point on the surface of the expansion nozzles can be obtained by knowing the local density in the inviscid flow. This can be derived from the pressure distribution on those surfaces. Integration over the surfaces then yields the drag due to skin friction on the expansion nozzles, in Newtons, as

$$4.8 \times 10^{-5}\ P_f .$$

The skin friction on the part of the model support sting exposed to the flow was estimated to be negligible.

10. RESULTANT FUEL-OFF DRAG

Fig. 13 displays the results of the above calculations, with eq(1) used to relate P_f to P_p. Fig. 13(a) shows the inviscid drag, as the drag due to the intake and the cowl, minus the

thrust due to the expansion nozzle. Ideally, it should be possible to design a model such that one largely cancels the other, apart from a relatively small effect due to entropy rise in the intake, and to the reduction in expansion nozzle area ratio occasioned by the need to support the model on the sting. The fact that the residual drag is not small is largely due to two effects. The first is the drag due to the cowl leading edge bevel, which was incorporated solely for ease of manufacture of the model, and the second is the limited thrust performance of the expansion nozzle. This is due partly because it is operating at combustor flow Mach numbers about 4, which, as shown by fig.12, is considerably in excess of the optimum value, and this entails a considerable reduction in thrust. It is also due to the fact that even at lower Mach numbers, its thrust performance could be improved, as shown by the comparison with a one-dimensional nozzle in fig. 12.

Fig. 13(b) shows the viscous drag. It can be seen that the drag divides approximately evenly between the combustion chambers, where the boundary layer is turbulent, and the intake plus the cowl exterior surface, where the boundary layer is laminar. The expansion nozzle makes a small contribution only. The total viscous drag is comparable with the inviscid drag which, as already mentioned, can be substantially reduced by good design to leave viscous drag as the dominant contribution. This illustrates the point that successful operation of scramjet vehicles will be heavily dependent on control of these viscous losses.

The inviscid drag and the viscous drag are combined to yield the resultant drag in fig. 13(c), where it is compared with measurements. The possible error in the measurements is about equally due to uncertainty in the measured drag and uncertainty in the measured

Pitot pressure. Within the limits of error, it is clear that theory and experiment agree, except for a tendency for the drag to increase somewhat more rapidly with stagnation enthalpy than is indicated by the theory. This could be due to the theoretical model used for turbulent skin friction.

11. INVISCID FUEL-ON THRUST

Combustion chamber pressure rise. The propulsive effect of a scramjet derives from the pressure rise experienced in the combustion chambers due to mixing and burning of the fuel there. If either, or both, of these processes are not completed in the combustion chamber the pressure rise is reduced, and therefore so is the thrust.

Shock tube data (Jackimowski & McLain 1983) indicates that, regardless of the presence of silane, the fuel should not burn in the combustion chambers. However shock tunnel experiments (Morris 1988) exhibit much shorter reaction lengths, due possibly to high boundary layer temperatures and "frozen" oxygen radicals in the freestream. Under the conditions of the present tests, reaction lengths of the order of 10 mm are likely, and as this is much less than the length of the combustion chambers it is assumed that complete combustion of all the fuel that is mixed takes place.

An indication that essentially complete mixing occurred was obtained by plotting the thrust obtained against the fuel equivalence ratio, as in fig. 14(a). It can be seen that the thrust varied approximately as the fuel mass flow, suggesting that the proportion of fuel burnt was approximately independent of the mass flow. Since the proportion of a fuel jet which is mixed in the length of combustion chamber will only be invariant with the jet

mass flow if all of the jet is mixed, it is reasonable to assume that complete mixing occurred.

Thus, an analysis was conducted of pre-mixed, equilibrium combustion in a constant area duct of the silane-hydrogen fuel. It was assumed that the silane burned according to the reaction

$$SiH_4 + 2O_2 \rightarrow SiO_2 + 2H_2O \ ,$$

and the hydrogen according to the reaction

$$2H_2 + O_2 \rightarrow 2H_2O \ .$$

Dissociation of H_2O in the combustion products was taken into account (e.g. Beniot 1968) and, since post combustion temperatures were above the condensation temperature of SiO_2, it was assumed to remain in the vapour state. The analysis was conducted in a conventional manner, using the energy equation, with the heats of formation included in the enthalpy, together with the momentum equation and the equation of state, applied across a shock-like discontinuity. The change in molecular weight due to addition of the fuel, and due to its chemical reaction with air, were taken into account. For each set of precombustion conditions, a solution was obtained iteratively, yielding the results shown in fig. 14(b). They show that the combustion heat release has a reducing effect as the stagnation enthalpy, and therefore the pre-combustion temperature, is increased. The combustion pressure rise is reduced, and the post-combustion Mach number increases, to come closer to pre-combustion values. A curve for the temperature ratio across the combustion zone is also presented, showing that the pressure rise is almost entirely due to the combustion temperature rise.

The effect of dissociation of H_2O in the combustion products on the temperature rise increased with stagnation enthalpy, reducing T_c by 6% at 3 MJ kg^{-1}, and 25% at 8.5 MJ kg^{-1}. Thus, at the higher stagnation enthalpy, dissociation reduced P_c/P_f from 1.5 to 1.2, which is not a large effect when compared with that of pre-combustion temperature. Hence, for the conditions of this paper, dissociation is not considered to be important.

The effect of combustion was measured by making a series of pressure tappings in one of the combustion chambers, as shown in fig. 15. Although the non-uniformity of the flow makes an exact comparison with the theory impossible, it can be seen that if the average of the two downstream data points is taken, the pressure level is predicted reasonably well. The upstream data points may be taken to indicate that mixing and/or combustion is not complete at those stations. As shown, Pitot pressure was also measured at a point which was just upstream of the expansion wave from the corner of the centrebody. Taking the mean of the static pressure at the two downstream stations when combustion occurred, and the ratio of specific heats for the combustion products, and combining these with the Pitot pressure, it was possible to obtain the Mach number of the flow after combustion. This varied from 1.5 to 2.2 as the stagnation enthalpy increased from 3.2 MJ kg^{-1} to 5.8 MJ kg^{-1}, signifying that supersonic combustion had indeed taken place.

Expansion Nozzles. The thrust due to the expansion nozzles is obtained as before with P_c replacing P_f as the pressure before expansion. The frozen ratio of specific heats for the combustion products differed from 1.4 by only 3%, so fig. 12 could be used again to predict the thrust. However, it should be noted that combustion reduces the Mach

number at the entrance to the nozzles, an effect which was taken into account by using the theoretically calculated Mach numbers presented in fig. 14.

Fuel Injection Thrust. There is a substantial amount of thrust associated with fuel injection, and to take account of this it was noted that the fuel supply duct pressure, P_F, was an order of magnitude greater than the pre-combustion pressures in the combustion chambers. Thus it was assumed that after injection, the fuel expanded to very low pressures. The velocity of the fuel could thus be obtained as $\sqrt{2/(\gamma-1)}\ a_F$, where a_F is the speed of sound in the fuel before injection, and by combining this with the fuel mass flow, and allowing for the injection angle, the thrust could be determined. A discharge coefficient of 0.9 was used for the fuel orifices, and for fuel mass flows corresponding to an equivalence ratio of 0.77, the thrust in Newtons was

$$(60 - 4.2\ H_s) \times 10^{-5}\ P_f.$$

where eq(1) can again be used to express P_f in terms of P_p. While this was not inconsistent with measurements of thrust before the test flow arrived, as seen in fig. 9, the accuracy of those measurements prevented a more definitive comparison.

The results of these calculations are presented in fig. 16(a), for an equivalence ratio corresponding to the mean value used in the experiments. The inviscid drag of the intake and cowl remains as before, but the pressure rise due to combustion allows the expansion nozzle to produce much greater thrust. When this is added to the fuel injection thrust it is sufficient to outweigh the inviscid drag over most of the range of enthalpies studied.

12. VISCOUS FUEL-ON DRAG

The injection of fuel does not, of course, influence the skin friction drag on the intake and cowl, but it does affect the skin friction in the combustion chambers and the expansion nozzles, through the effect of combustion on the temperature of the flow external to the boundary layer. The theory of Spalding and Chi is used once again to yield

$$(70 - 3.0\ H_J) \times 10^{-5}\ P_f$$

for the skin friction drag, in Newtons, on the combustion chambers under the calculated flow conditions. The skin friction drag on the expansion nozzles is also estimated according to the same approximation as in the fuel-off case, to yield, in Newtons,

$$6.3 \times 10^{-5}\ P_f\ .$$

These results are presented in fig.16(b) in terms of P_p. Comparison with fig. 13(b) reveals that the major change in skin friction drag associated with fuel injection is the increase in drag of the combustion chambers. This amounts to a 90% increase at a stagnation enthalpy of 3 MJ kg^{-1}, where the combustion has the largest proportional effect on the temperature. However, at 8 MJ kg^{-1}, where the proportional increase in temperature is greatly reduced, the increase in combustion chamber skin friction is only 14%.

The skin friction in the expansion nozzles is also increased, but this is such a small contribution to the overall skin friction drag that the magnitude of the increase can barely be noticed on the scale of fig. 16(b).

13. RESULTANT FUEL-ON AXIAL FORCE

The curves in fig. 16 for total inviscid axial force, and total viscous drag, are combined into one curve for the resultant axial force in fig. 17. In order to finally emphasise the propulsive performance, the curve is presented with thrust as the positive ordinate. Measurements of thrust are also presented, for fuel equivalence ratios near the value used in the theoretical calculations, and are seen to follow the theoretical predictions reasonably closely, with a tendency to fall below the theoretical curve at the higher values of stagnation enthalpy. This follows the same trend as for the fuel-off case, and to facilitate the comparison, the resultant drag curve and the measurements of fig. 13(c) are presented again in fig. 17. It seems likely that the cause of the discrepancy is the same in both areas.

It will be noted that the maximum thrust is obtained at the lowest stagnation enthalpy. Attempts to increase the maximum value achieved, either by lowering the stagnation enthalpy or by increasing the fuel equivalence ratio, produced unsteadiness in the force measurement and then "choking" of the flow through the model. In view of the low value ($\sim$ 1.5) measured for the post combustion Mach number at a stagnation enthalpy of 3.2 MJ kg^{-1}, it seems reasonable to conclude that this was due to thermal choking of the flow in the combustion chambers.

The propulsive performance of the model used in these experiments was not outstanding. For example, if the maximum value of thrust obtained is taken as $10 \times 10^{-5} P_p$ Newtons, the corresponding specific impulse is 175 sec. If the silane in the fuel were replaced by an amount of hydrogen sufficient to consume the same amount of oxygen, and the same

thrust were obtained, the fuel specific impulse would be 370 sec. However, it is worthwhile reiterating that the model was designed for ease of manufacture and analysis, and not for optimum performance.

Inspection of figs. 13 and 16 suggest ways in which the performance might be improved. Fig. 13(a) indicates that the inviscid drag of the configuration could be reduced; for example, by removing the external bevel on the cowl leading edges. The thrust delivered by the expansion nozzles could be improved by better design, although it must be remembered that combustion lowers the Mach number of the flow entering the expansion nozzles, and as shown in fig. 12 this improves the efficiency of the nozzles. Also expansion nozzles of larger area ratio would deliver more thrust, though provision of a larger expansion area ratio would impact other aspects of the overall design.

The viscous drag, as shown in figs. 13(b) and 16(b), represents a substantial portion of the overall drag, and one which offers less opportunity for reduction. However, there is a clear benefit in this respect in reducing the length of the combustion chambers, provided this can be done without reducing the benefits of combustion.

The relatively large size of the viscous drag points to one of the major difficulties associated with air breathing propulsion at very high speeds. It is likely to be an intractable form of drag, difficult to design against, and its importance here confirms the widely held view that it may be a major impediment to effective propulsion at such speeds.

Figs. 16 and 17 display the rapid decrease in net thrust which is occasioned by increasing stagnation enthalpy. This is, of course, due to the increasing combustor temperature before combustion, which reduces the combustion pressure rise. For application to an acceleration vehicle, a scramjet must operate near its optimum over a range of stagnation enthalpies, and therefore a means of maintaining the temperature before combustion reasonably constant would need to be found.

14. CONCLUSION

Thrust and drag measurements have been made in a shock tunnel on a supersonic combustion ramjet model. The effect of stagnation enthalpy on the propulsive performance of the model was measured for a range of stagnation enthalpies corresponding to flight velocities up to approximately 4 km/sec. A stress wave force balance was used, which involved monitoring the stress waves produced by the forces on this model as they passed into the model sting support. This, in combination with a pulsed fuel injection system, made the measurements possible.

The results were compared with theoretical predictions, and were found to be in generally good agreement, with a tendency to slightly underestimate the drag at high enthalpies. The analysis leading to the predictions involved the use of established theories which, together with some reasonable simplifying assumptions, provided estimates of the relative importance of the factors affecting the thrust and drag. Except for the combustion process itself, the analysis assumed a perfect gas with a ratio of specific heats of 1.4.

The experimental validation of this relatively simple theoretical analysis may be expected

to have a number of consequences. As well as indicating the significance of factors such as expansion nozzle performance and skin friction drag, it allows the benefits of concepts for improving the propulsive performance to be quantified, and thereby assists in improving the performance. Also, as with any flight vehicle, a simple analysis based on results of model experiments in a wind tunnel is useful for preliminary estimates of performance. Thus, with proper attention to factors such as the location of transition, estimates may be made of the performance of a scramjet powered vehicle in flight.

Using the theory, it was possible to identify areas where improvement may be expected to yield a gain in the overall thrust. For acceleration vehicles, it is clearly of primary importance that a means should be found of maintaining the precombustion temperature constant as the flight velocity changes. For cruise propulsion, this is less important. In general the inviscid drag of the configuration could be reduced by attention to design details and the performance of the expansion nozzles could be enhanced by matching them to the Mach number at which they are expected to operate. The theory also revealed the importance of viscous drag, and drew attention to the value of reducing viscous drag by reducing combustion chamber length.

However, perhaps the most important result is that the investigation has established a method for experimental testing of scramjet powered models at high velocities, together with the theoretical understanding which attends the approximate analysis. These two factors together may be expected to assist in the development of scramjet research.

ACKNOWLEDGMENTS

This work was supported by the Australian Research Council and by the National Aeronautics and Space Administration, U.S.A. under grant NAGW-674.

REFERENCES

Anderson, D.A. & Nangia, R.K. 1977 "Comparison of Numerical and Experimental "Conical" Flow Fields in Supersonic Corners with Compression and/or Expansion" Aeronautical Quarterly, 28, 293.

Benoit, A. 1968 "Equilibrium Thermodynamic Data for the H_2-O_2-He System" Univ. of Toronto, Institute for Aerospace Studies. Tech. Note. No. 128.

Bernstein, L. & Stott, G.T. 1982 "A Laser-Interferometer Method for Determining the Forces on a Freely Flying Model in a Shock Tunnel" Aero. Quarterly, 23, 237.

Billig, F.S. 1993 "Research on Supersonic Combustion" J. of Propulsion & Power, 9, 449.

Ferri, A. 1964. "Review of Problems in Application of Supersonic Combustion" J. of Royal Aero. Soc., 68, 575.

Hall. N.A. 1951 "Thermodynamics of Fluid Flow" pp. 112-114 New York: Prentice-Hall.

Hayes, W.D. & Probstein, R.F., 1959 "Hypersonic Flow Theory" p.296. New York: Academic Press.

He, Y. & Morgan, R.G. 1994 "Transition of Compressible High Enthalpy Boundary Layer Flow over a Flat Plate" The Aero. Journal, 98, 25.

Hopkins, E.J. & Inouye, M. 1971 "An Evaluation of Theories for Predicting Turbulent Skin Friction and Heat Transfer on Flat Plates at Supersonic and Hypersonic Mach Numbers" AIAA J. 9, 933.

Jackimowski, C.J. & McLain, A.G. 1983. "A Chemical Kinetic Mechanism for the Ignition of Silane/Hydrogen Mixtures" NASA TP2129.

Jessen, C. & Grönig, H. 1989 "A New Principle for a Short-Duration Six Component Balance" Experiments in Fluids, 8, 231.

Jones, R.A. & Huber, P.W. 1978 "Towards Scramjet Aircraft" Astronautics & Aeronautics, 16, 38.

Lordi, J.A., Mates, R.E. & Moselle, J.R. 1966 "Computer Program for Numerical Solution of Non-equilibrium Expansion of Reacting Gas Mixtures" NASA CR-472.

Morris, N.A. 1988 "Silane as an Ignition Aid in Scramjets" M.Eng.Sc. Thesis, Dept. of Mechanical Engineering, The Univ. of Queensland.

Narashima, R. & Viswandth, P.R. 1975 "Reverse Transition of an Expansion Corner in Supersonic Flow" AIAA J, 13, 693.

Naumann, K.W., Ende, H., Mathiew, G. and George, A. 1993 "Millisecond Aerodynamic Force Measurement with Side-Jet Model in the ISL Shock Tunnel" AIAA J. 31, 1068.

Porter, L.M., Paull, A., Mee, D.J. & Simmons, J.M. 1994 "Shock tunnel measurements of hypervelocity blunted cone drag" Accepted for publication AIAA J, April, 1994.

Prost, R. & Goutte, R. 1984 "Discrete constrained iterative deconvolution algorithms with optimised rate of convergence", Sig. Proc. 7, 209-230.

Sanderson, S.R. & Simmons, J.M. 1991 "Drag Balance for Hypervelocity Impulse Facilities, AIAA J. 29, 2185.

Simmons, J.M., Daniel, W.J., Mee, D.J. & Tuttle, S.L. 1993 "Force Measurement in

Hypervelocity Impulse Facilities" New Trends in Instrumentation for Hypersonic Research (ed A. Boutier) p.285. Kluwer Academic Publishers, Dordrecht.

Stalker, R.J. & Morgan, R.M. 1984 "Supersonic Hydrogen Combustion with a Short Thrust Nozzle" Combustion & Flame, 57, 55.

Swithenbank, J. 1967 "Hypersonic Air-breathing Propulsion" Progress in the Aeronautical Sciences, (ed. D. Küchemann). Pergamon, Oxford, 2, 229.

Tuttle, S.L. 1990 "A Drag Measurement Technique for Hypervelocity Impulse Facilities" M.Eng.Sc. thesis, Dept. of Mechanical Engineering, The Univ. of Queensland.

LIST OF FIGURES

Fig 13. Drag Without Fuel Injection. ——— theory, ⊡ experiment.

H_s = stagnation enthalpy
(a) Inviscid Drag
(b) Viscous Drag
(c) Resultant Drag.

Fig 14. Combustion Features
(a) Experimental effect of fuel mass flow.
(b) Theoretical effect of combustion.
ΔF = thrust increment due to fuel injection, ϕ = equivalence ratio, P_c = post combustion pressure, T_c = post combustion temperature, M_c = post combustion Mach number, H_s = stagnation enthalpy.

Fig 15. Combustion Chamber Pressures
Fuel-off: ○ Experiment, – – – – – theory.

Fuel-on: △ Experiment, —— theory (ϕ = 0.77)

H_s = stagnation enthalpy.

Fig 16. Axial Force with Fuel Injection and Combustion
Equivalence ratio ϕ = 0.77, F_A = axial force (+ve for thrust),
H_s = stagnation enthalpy
(a) Inviscid axial force
(b) Viscous Drag

Fig 17. Resultant Axial Force
Fuel-on: Equivalence ratio ϕ - 0.77 ± 0.10

▽ Experiment, —— theory.

Fuel-off: □ Experiment, — theory.

F_A = axial force, P_p = Pitot pressure, H_s = stagnation theory.

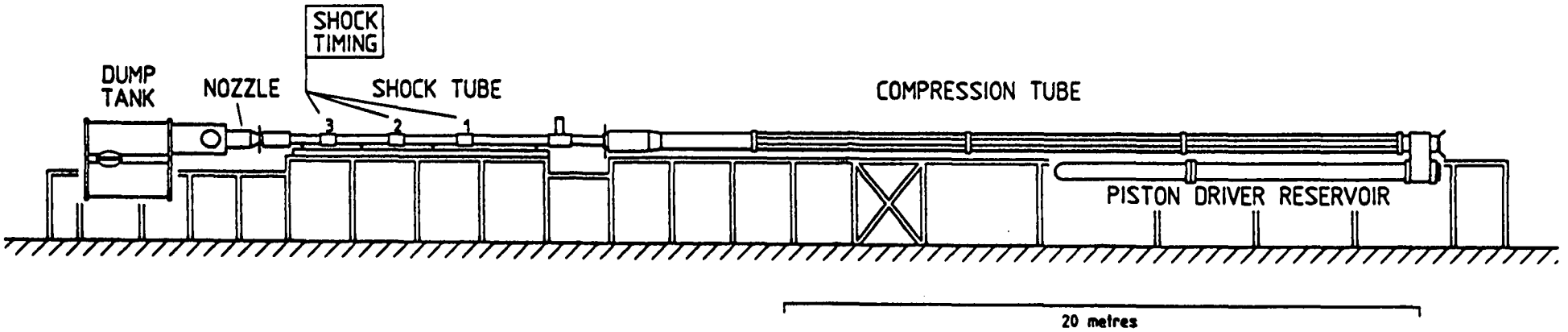
SHOCK
TIMING
DUMP
TANK
NOZZLE
SHOCK TUBE
COMPRESSION TUBE
3
2
1
PISTON DRIVER RESERVOIR
20 metres

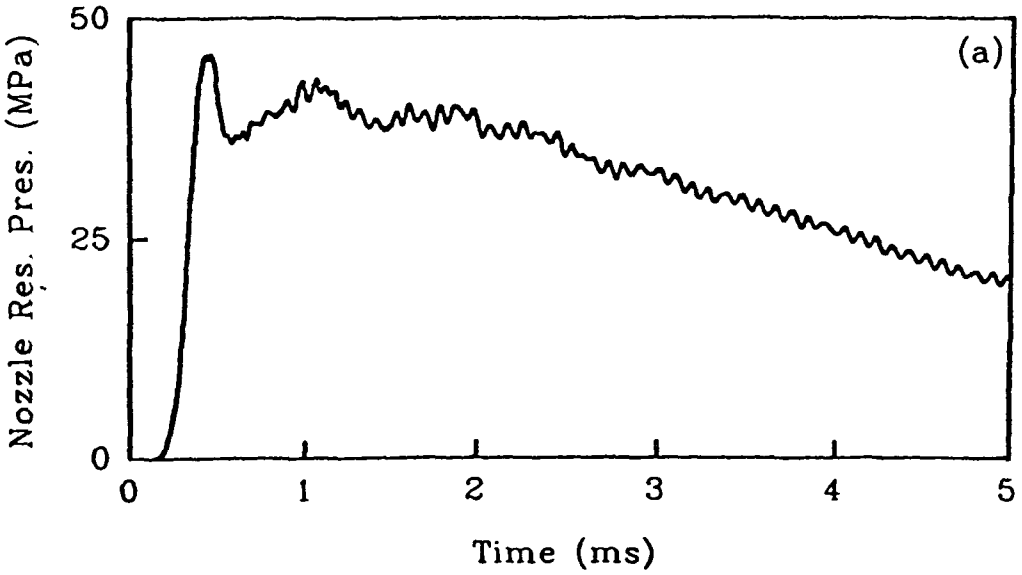
50
25
0
Nozzle Res. Pres. (MPa)
(a)
0
1
2
3
4
5
Time (ms)

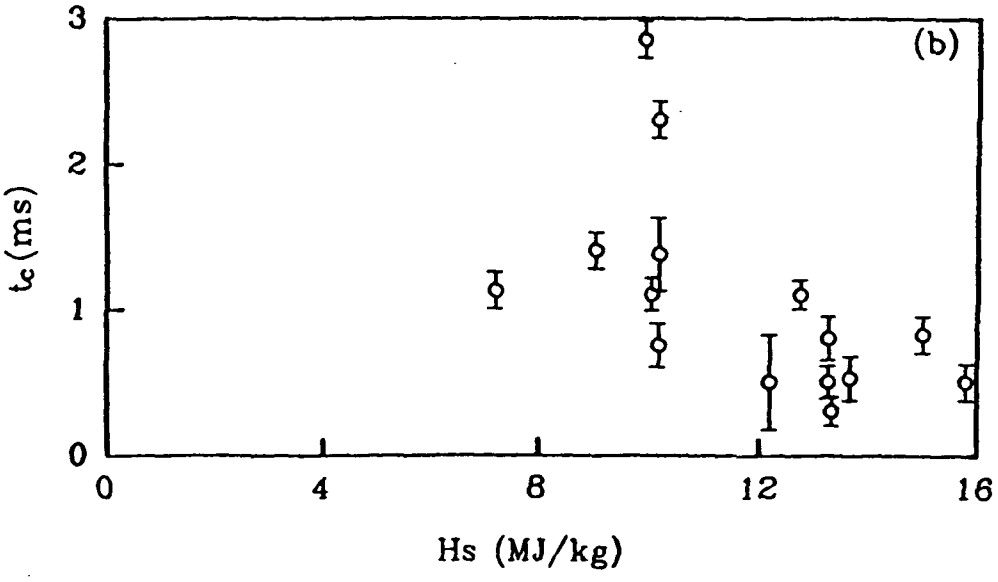
3
2
1
0
t_c (ms)
(b)
0
4
8
12
16
Hs (MJ/kg)

Fig 2

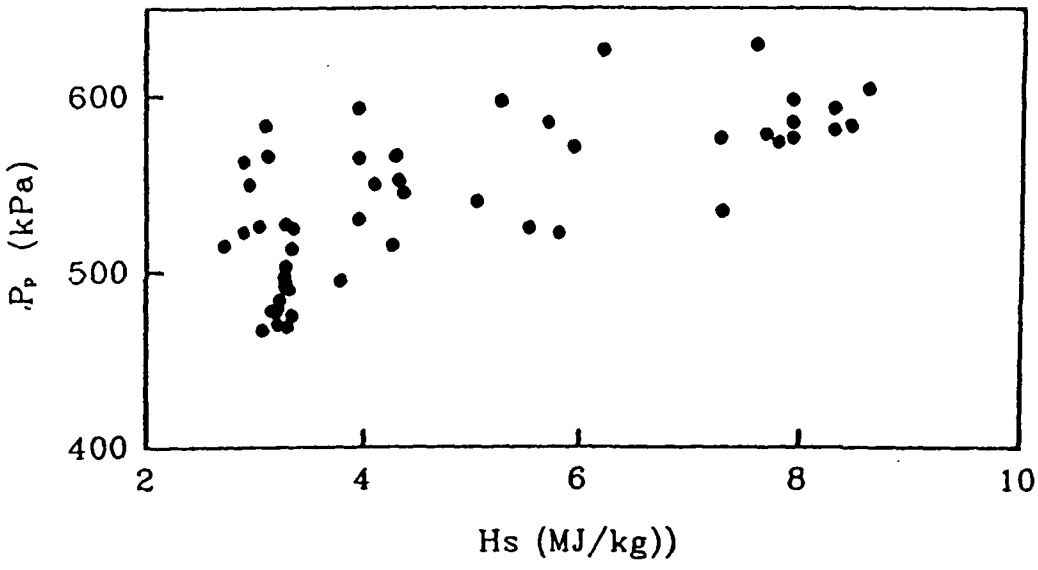

(a) Measured Pitot Pressure

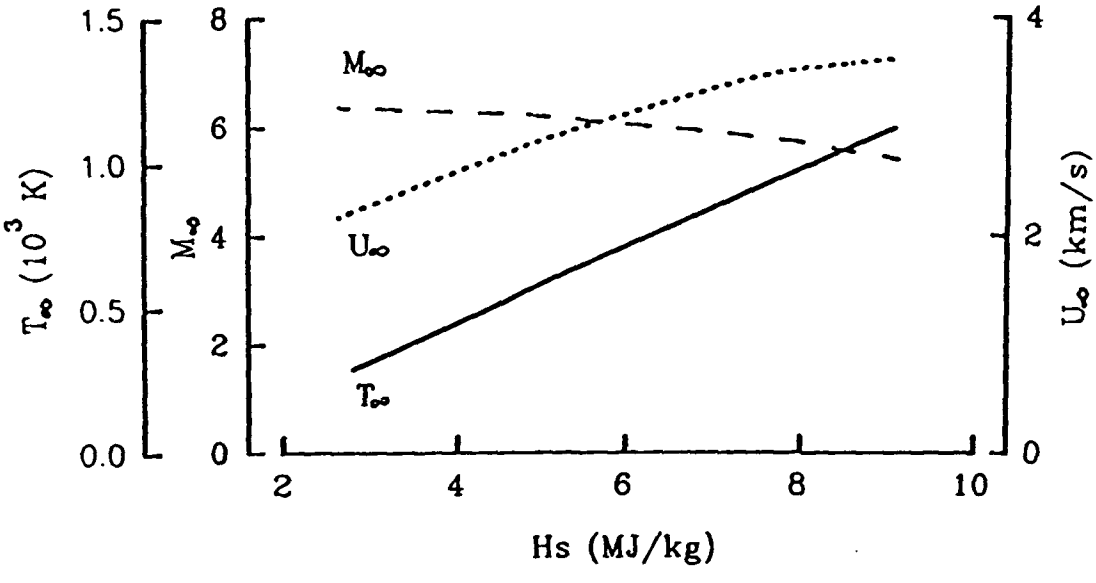

(b) Calculated Conditions

Fig 3

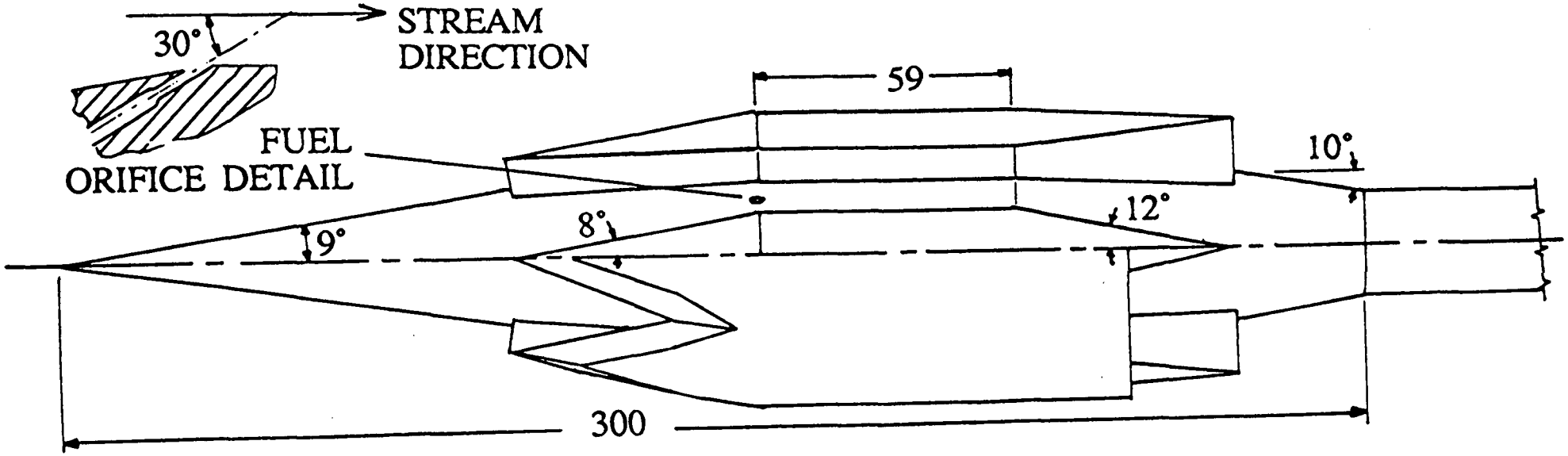

Fig 5. The scramjet model

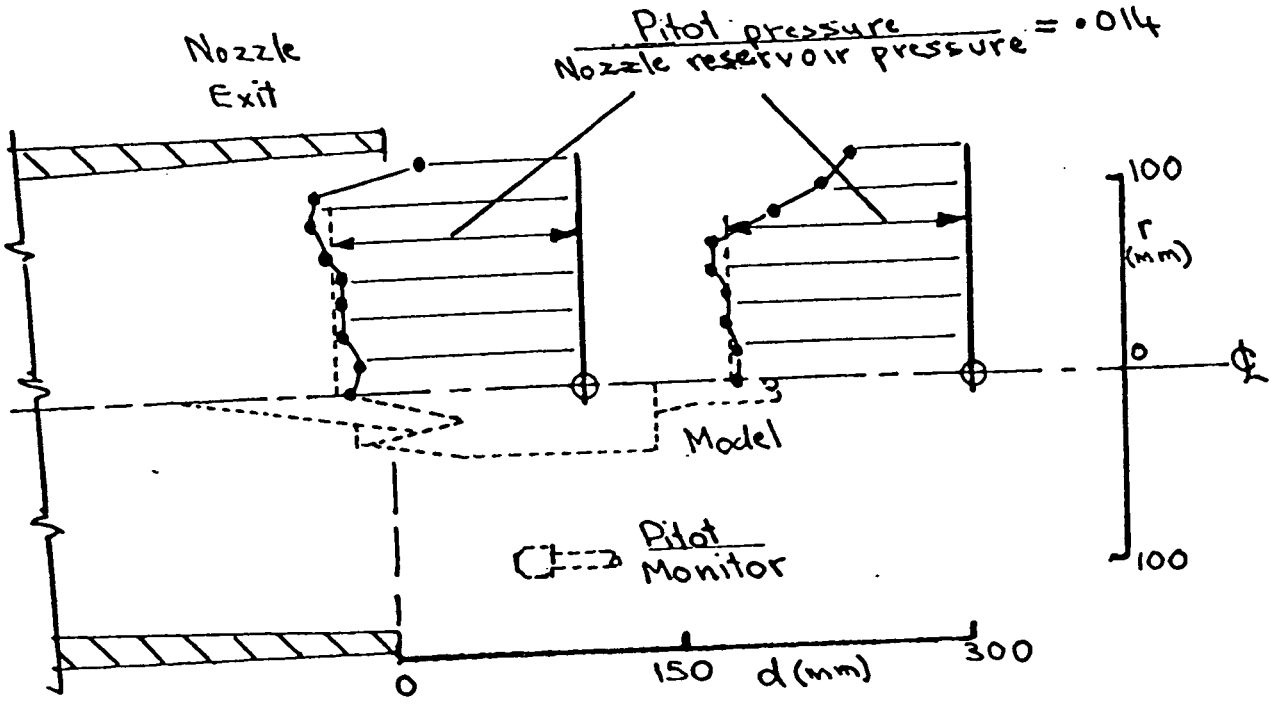

Fig 4. Test Section Flow Calibration and Location of Model. Stagnation enthalpy 8 $MJ.kg^{-1}$.

• Pitot survey measurements, d = downstream distance from nozzle exit, r = distance from centreline

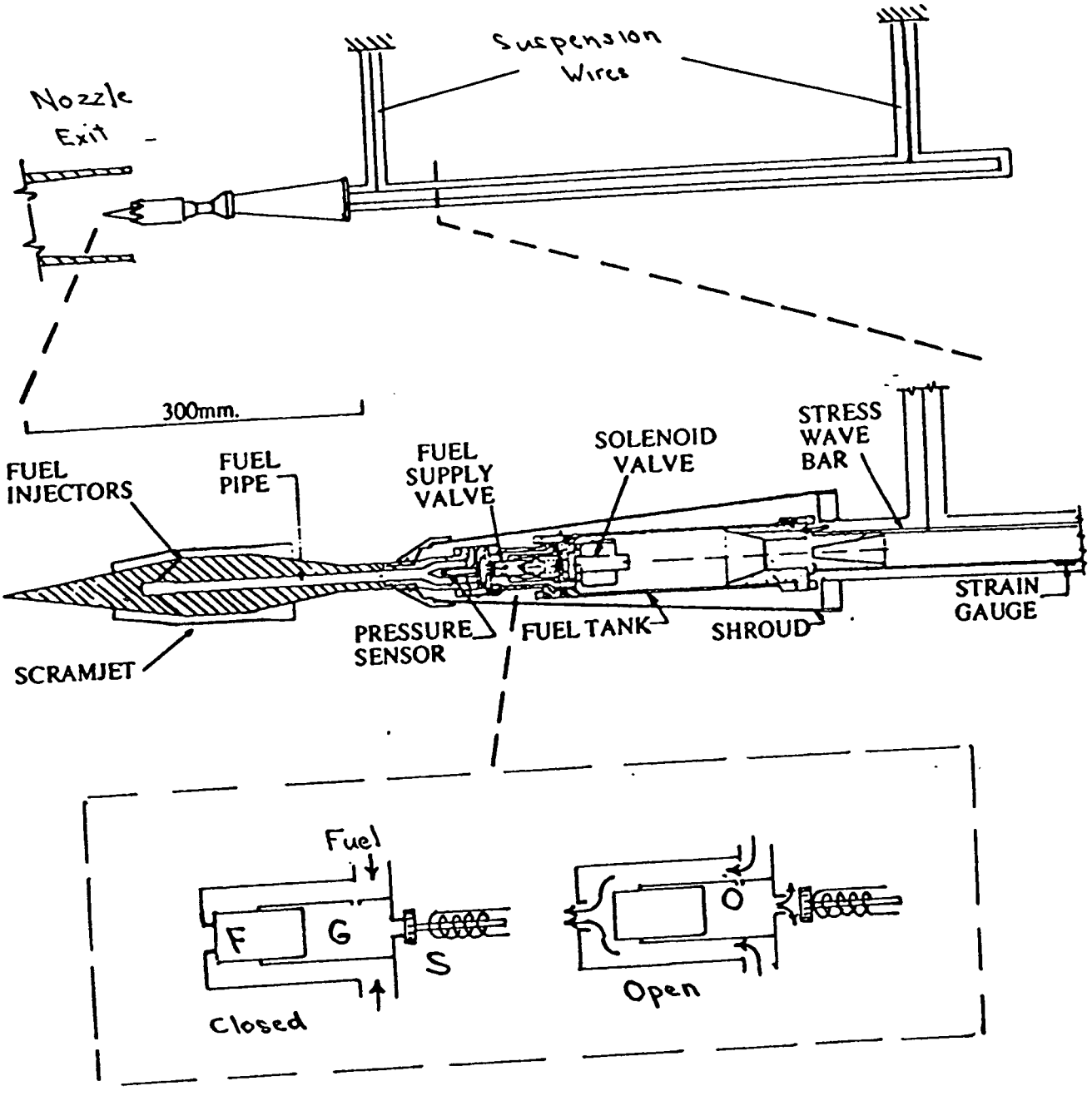

Fig 6. Model, Fuel Supply System and Model Mount

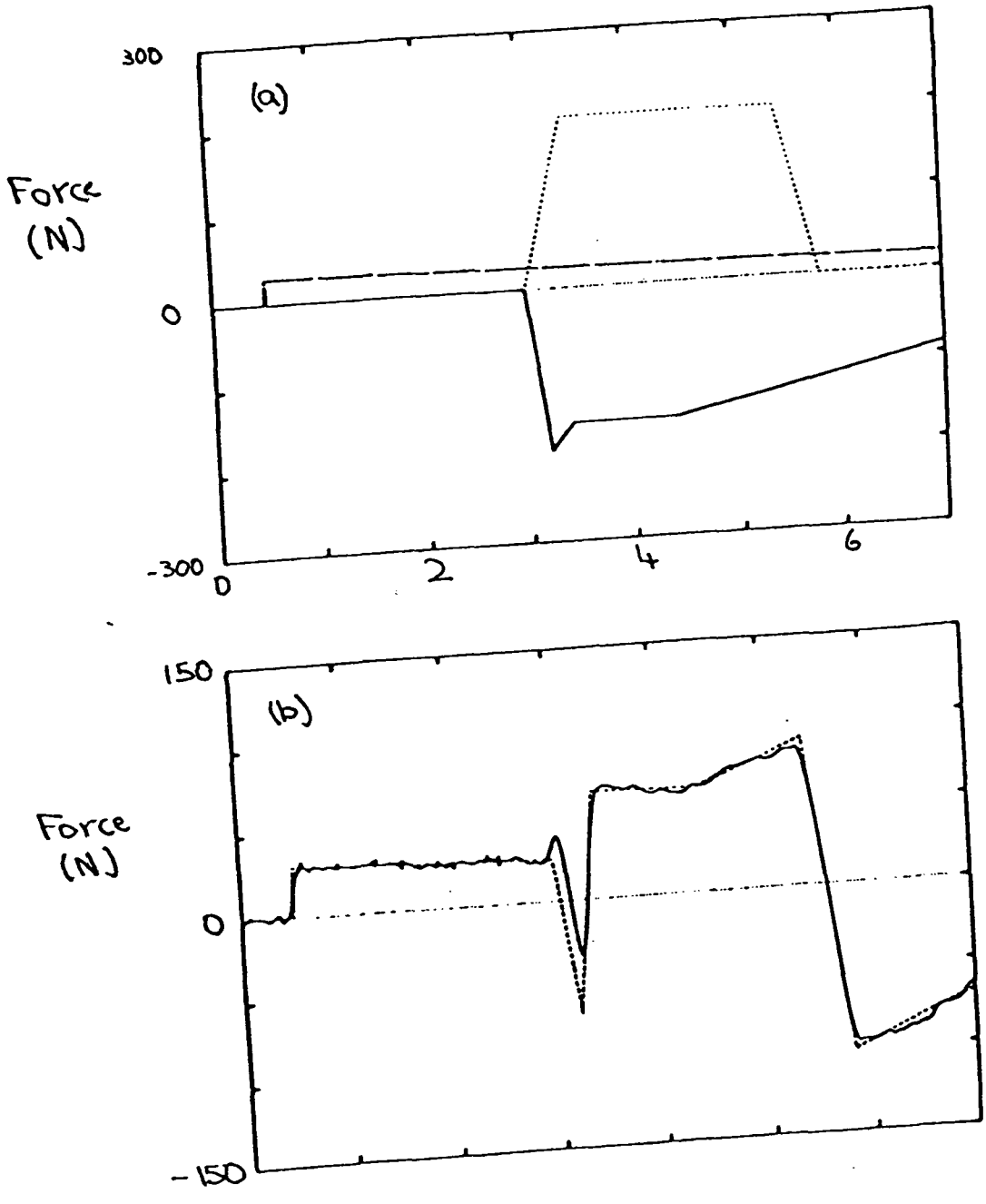

Fig 7. Simulation of Distributed Load (a) Input loads
— — fuel injection —— Drag ------ Thrust.
(b) Output. —— deconvolved load ---- true input.

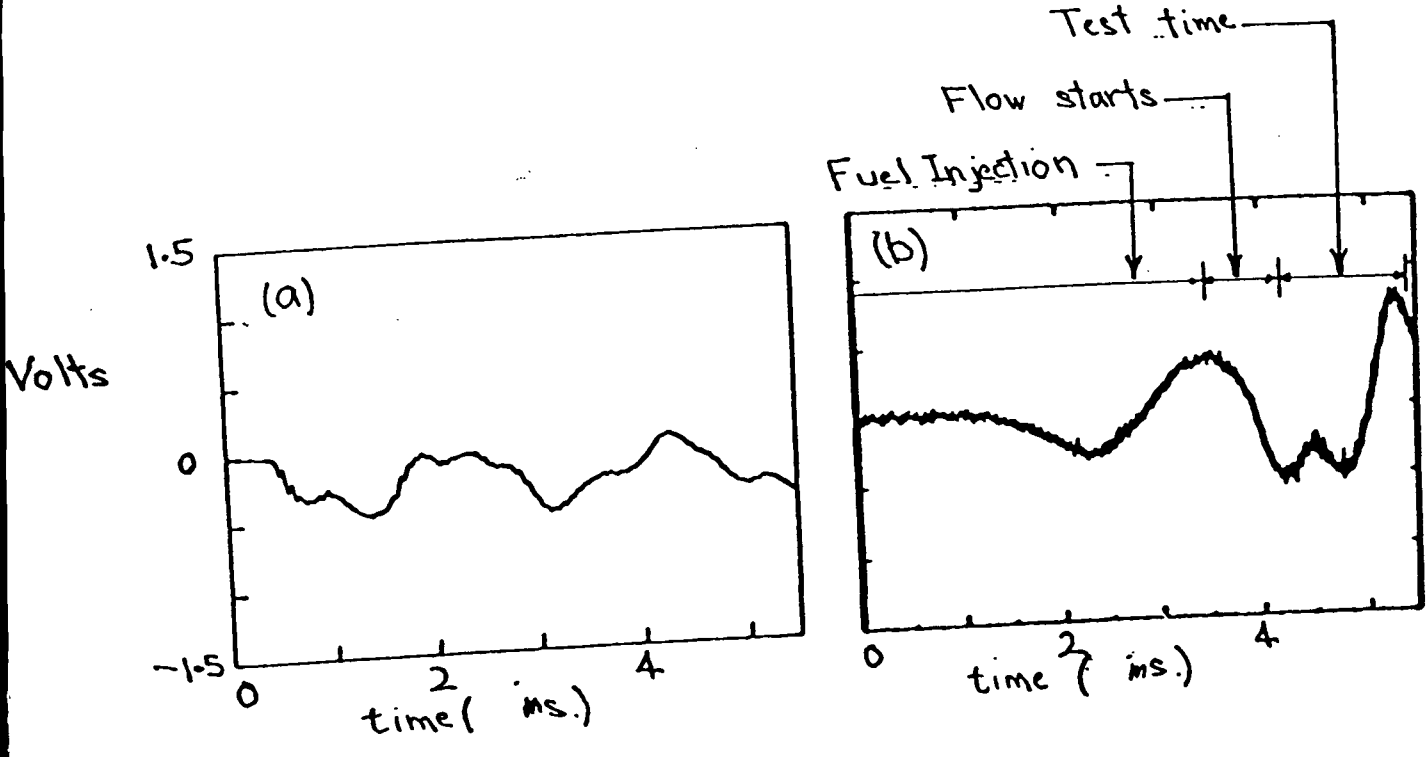

Fig 8 Strain Gauge Outputs (a) Response to step load
(b) Response during test

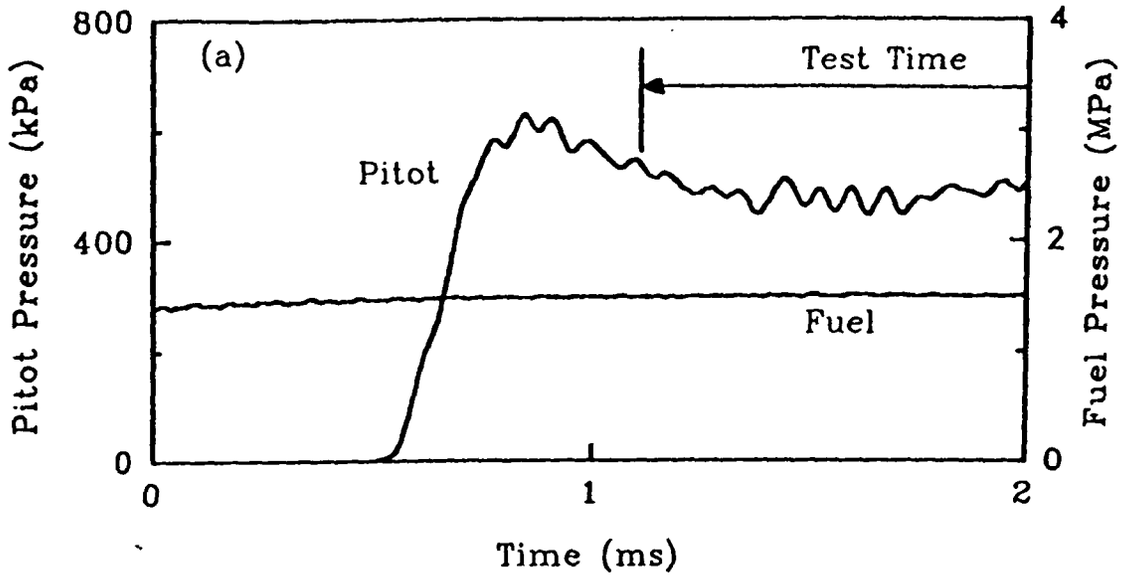
(a)
Test Time
Pitot
Fuel
800
400
0
4
2
0
0
1
2
Pitot Pressure (kPa)
Fuel Pressure (MPa)
Time (ms)

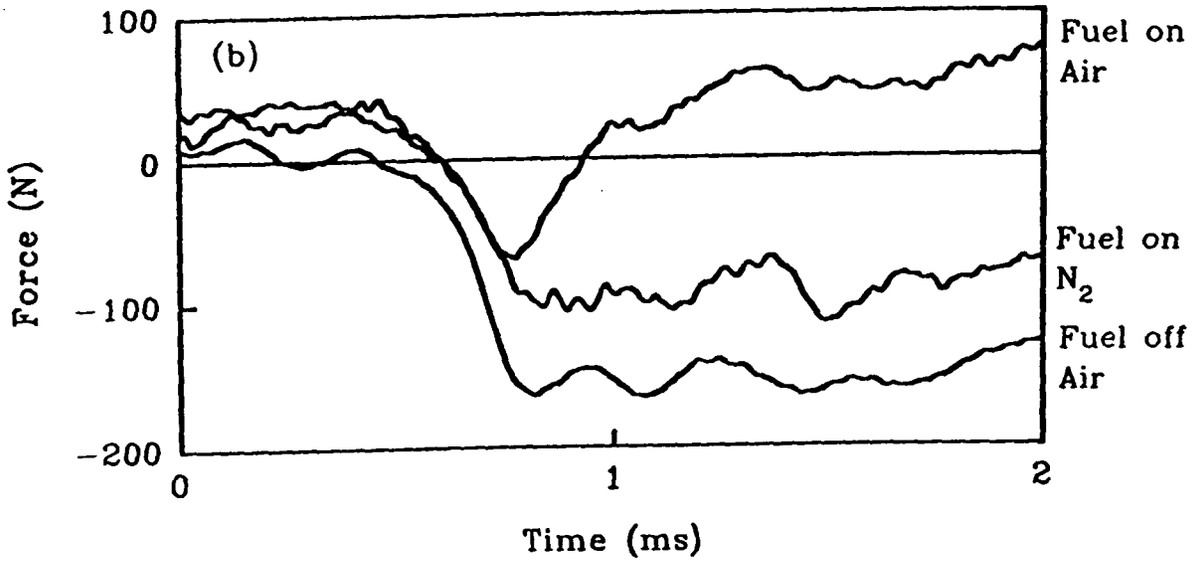
(b)
Fuel on Air
Fuel on N_2
Fuel off Air
100
0
−100
−200
0
1
2
Force (N)
Time (ms)

Fig 9 a/b

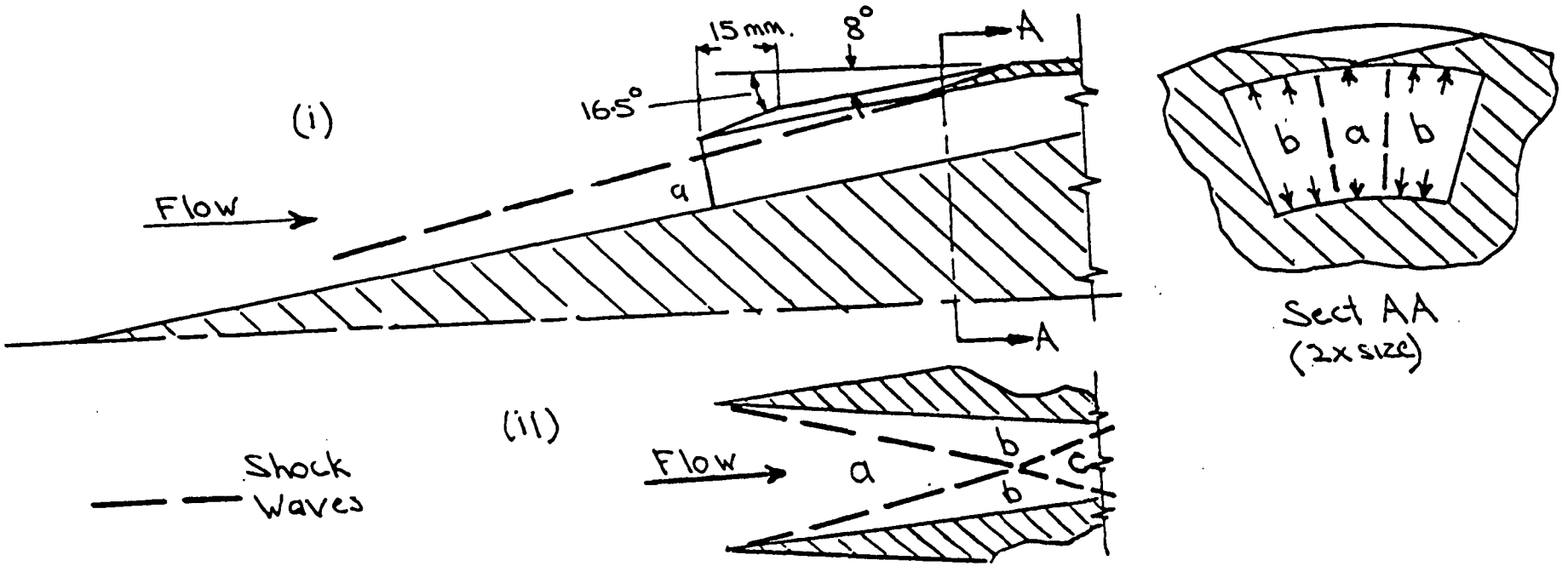

Fig 10. Intake Flow (i) Forecone and Inlet Cowl
(ii) Shock pattern between Splitters.

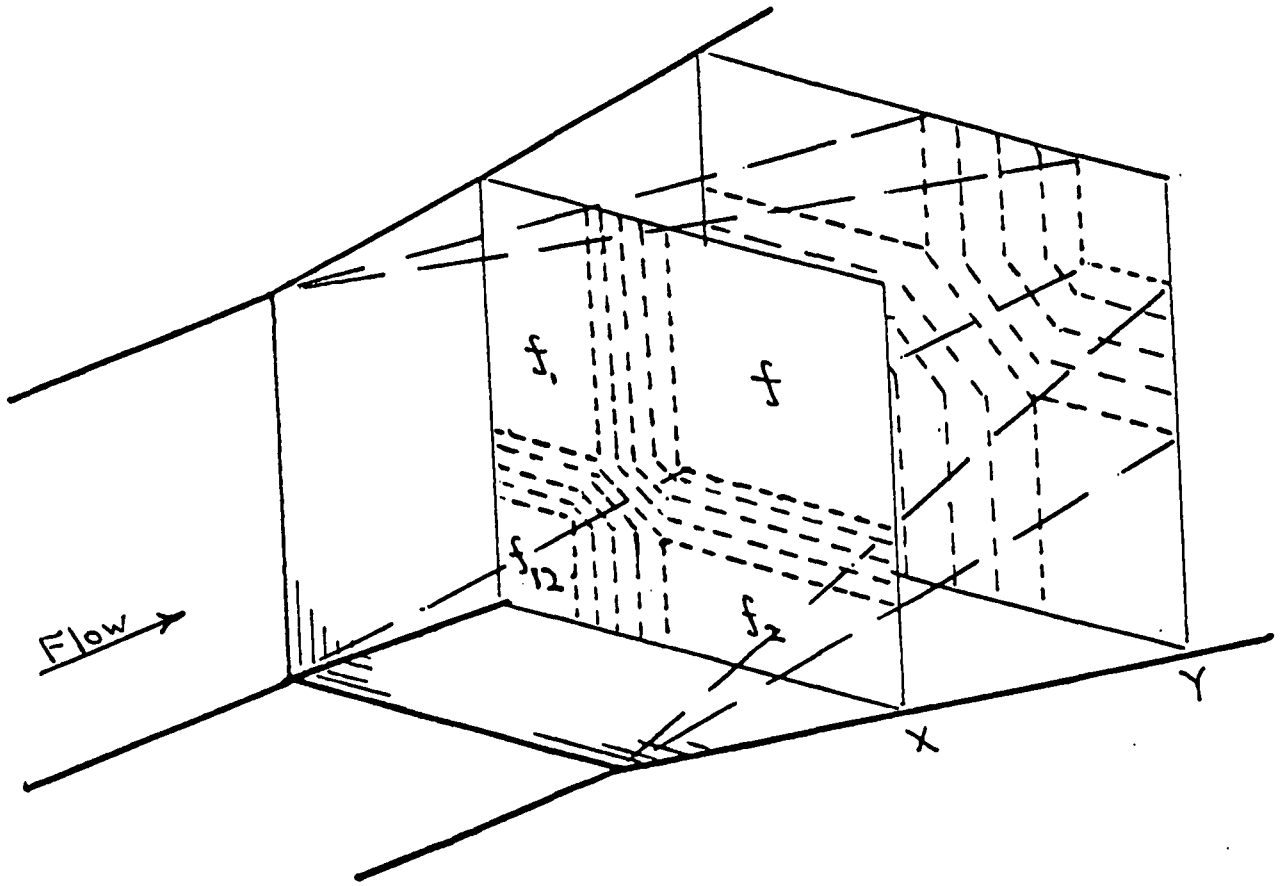

Fig 11. Expansion Nozzle Flow

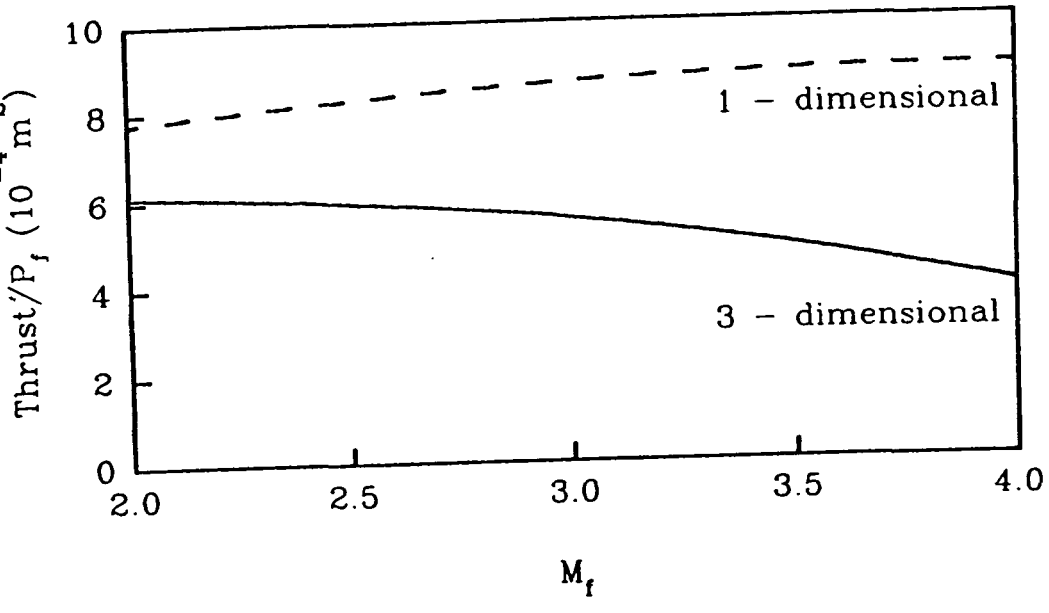
10
8
6
4
2
0
2.0
2.5
3.0
3.5
4.0
Thrust/P_f (10^{-4} m^2)
M_f
1 – dimensional
3 – dimensional

Fig 12

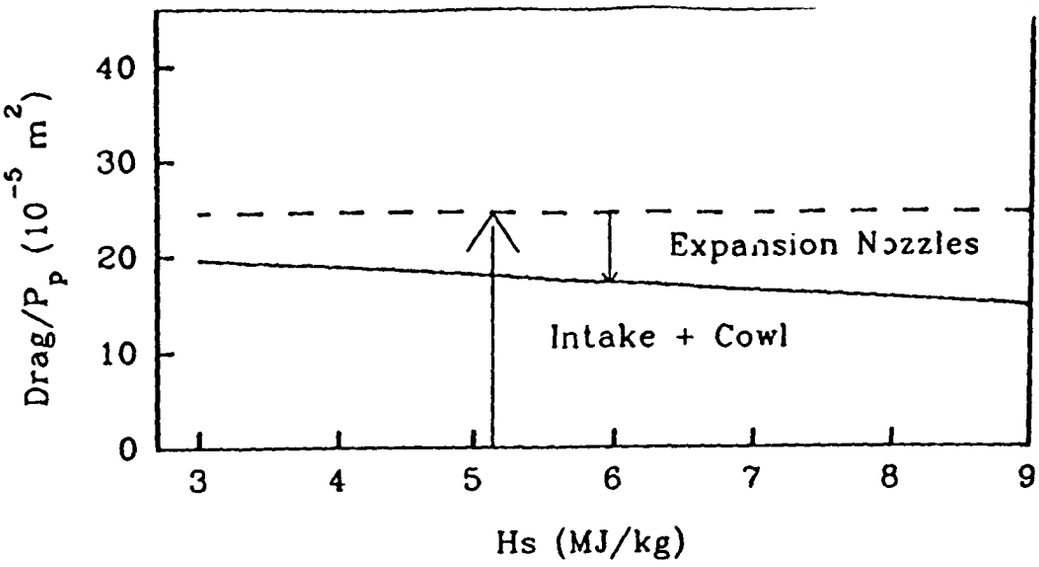

(a) Inviscid Drag

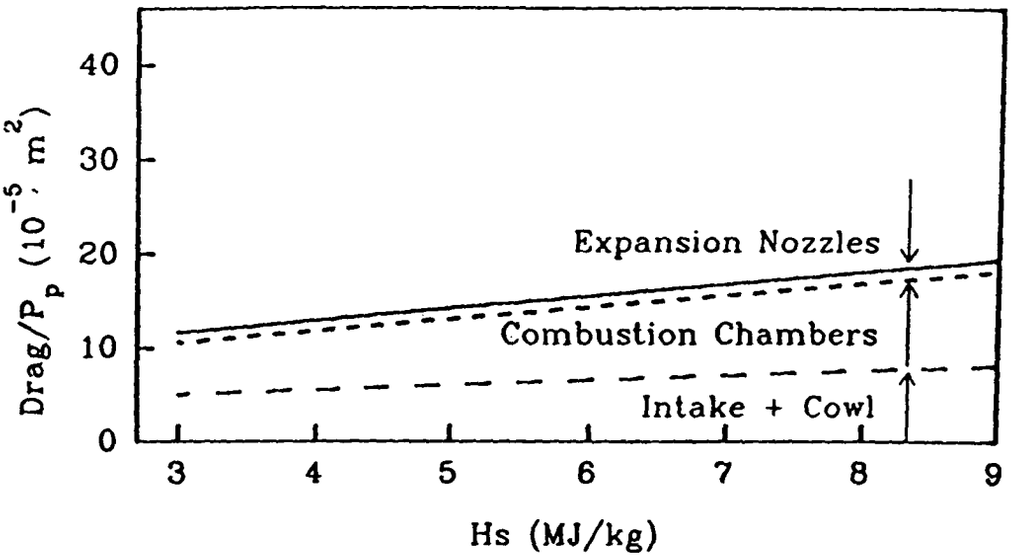

(b) Viscous Drag

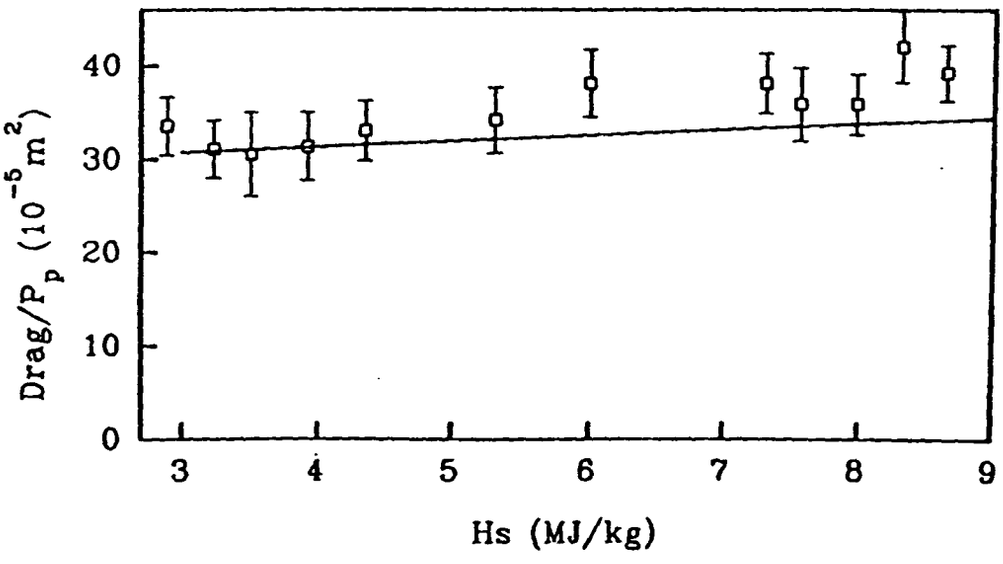

(c) Resultant Drag

Fig 13

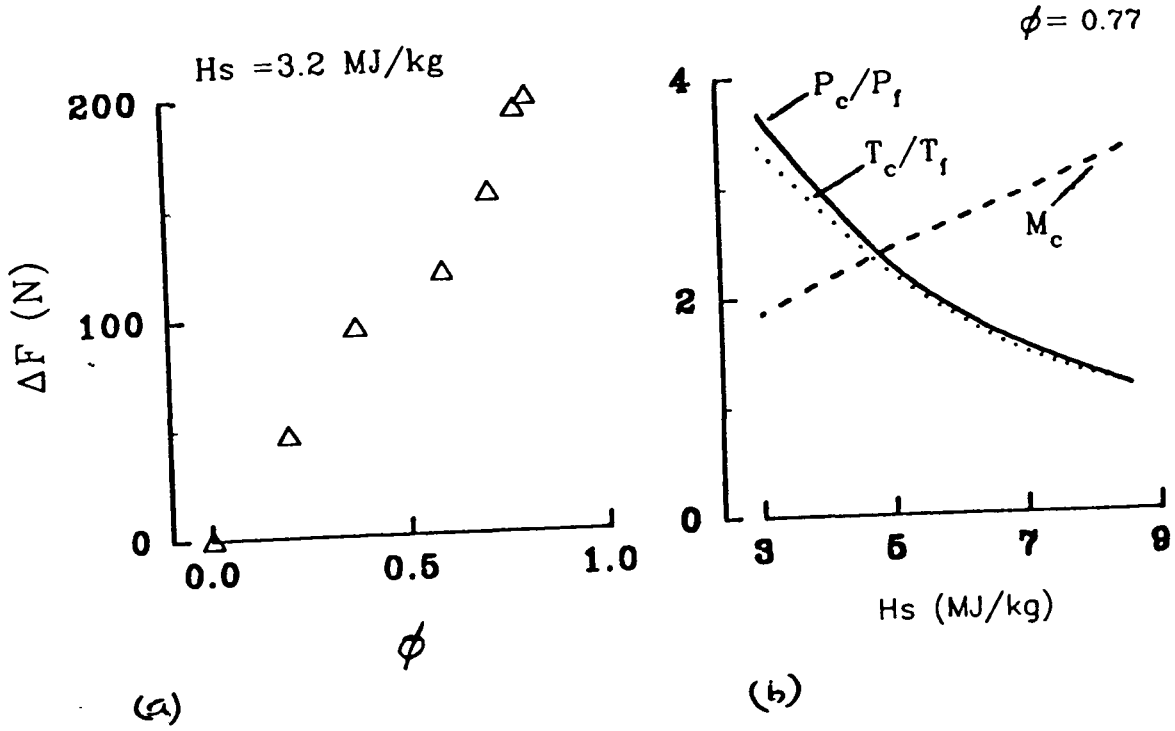
Hs =3.2 MJ/kg
200
100
0
ΔF (N)
0.0
0.5
1.0
φ
(a)
φ= 0.77
4
2
0
P_c/P_f
T_c/T_f
M_c
3
5
7
9
Hs (MJ/kg)
(b)

Fig 14

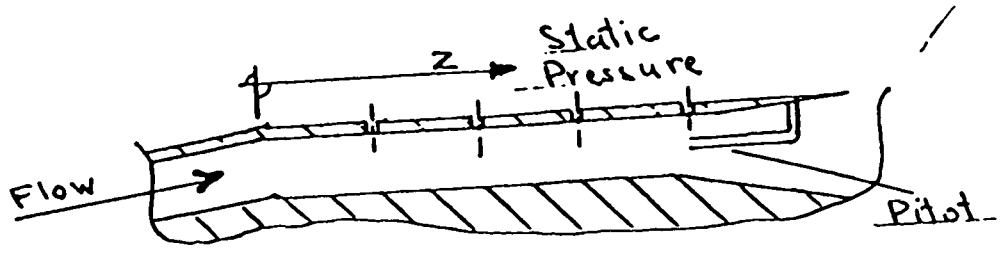

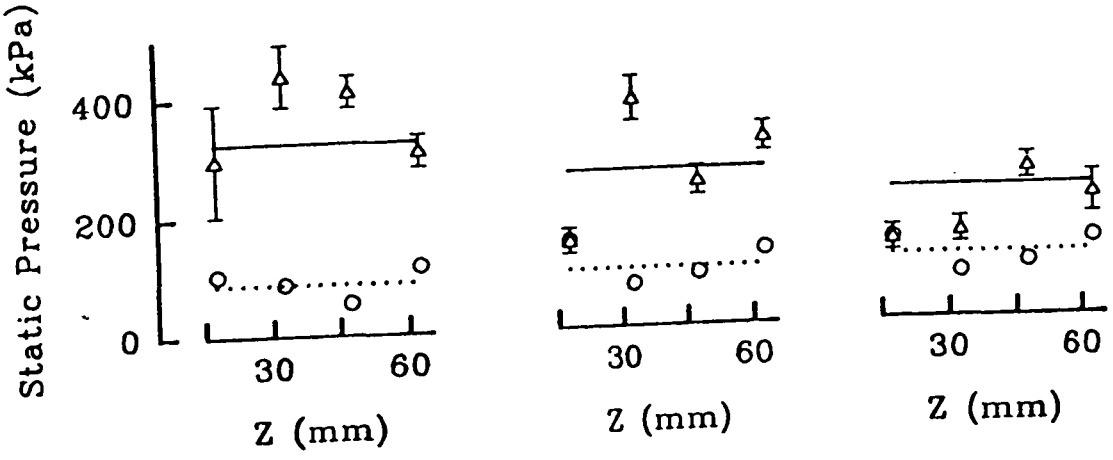

Hs (MJ/kg) 3.2 4.3 5.5

Fig

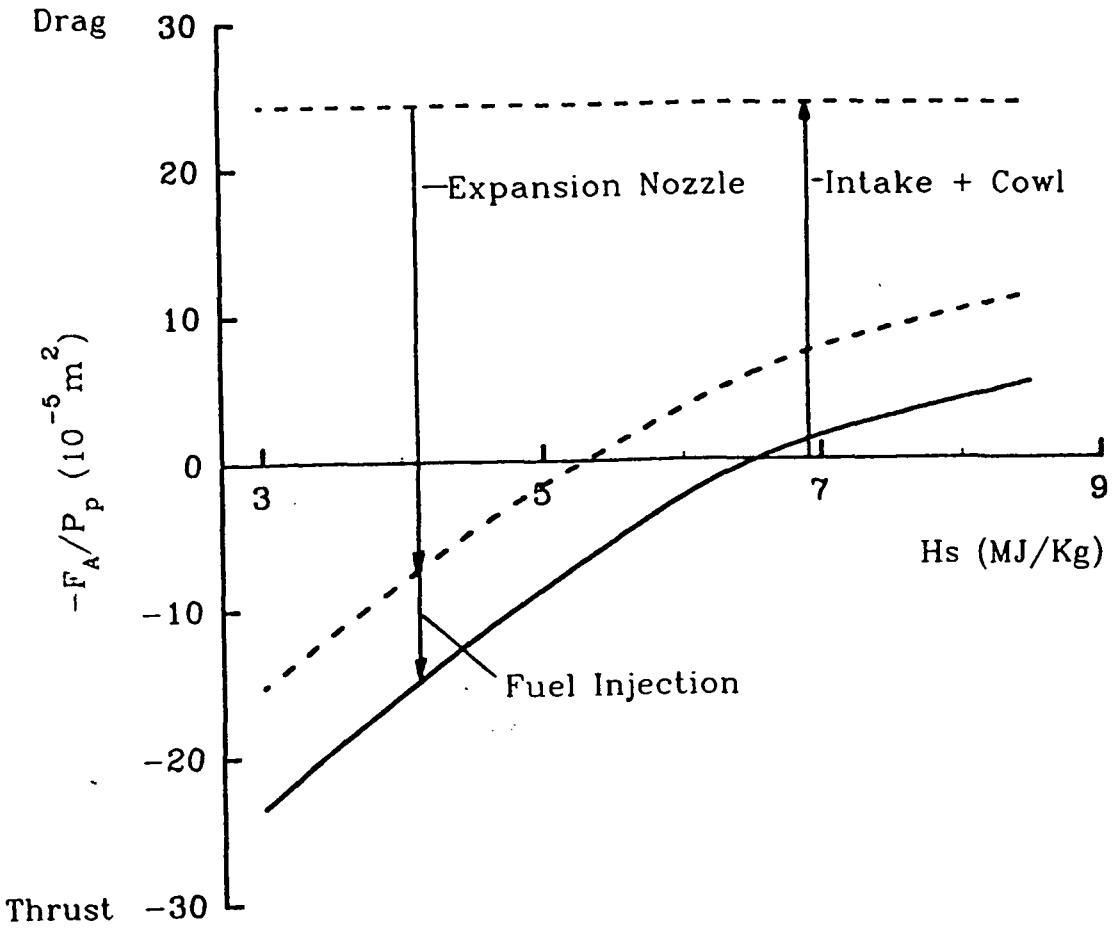

(a) Inviscid Axial Force

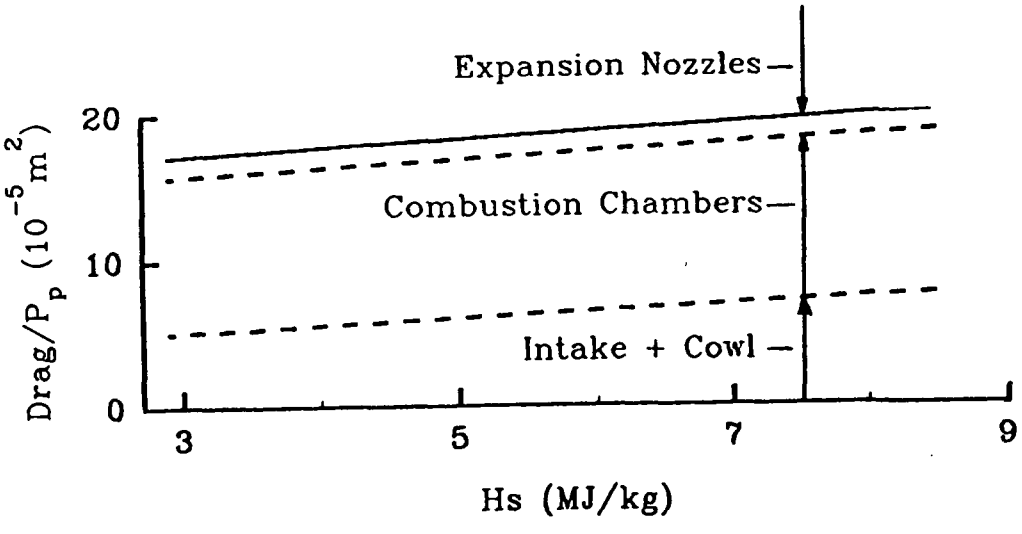

(b) Viscous Drag

Fig 16

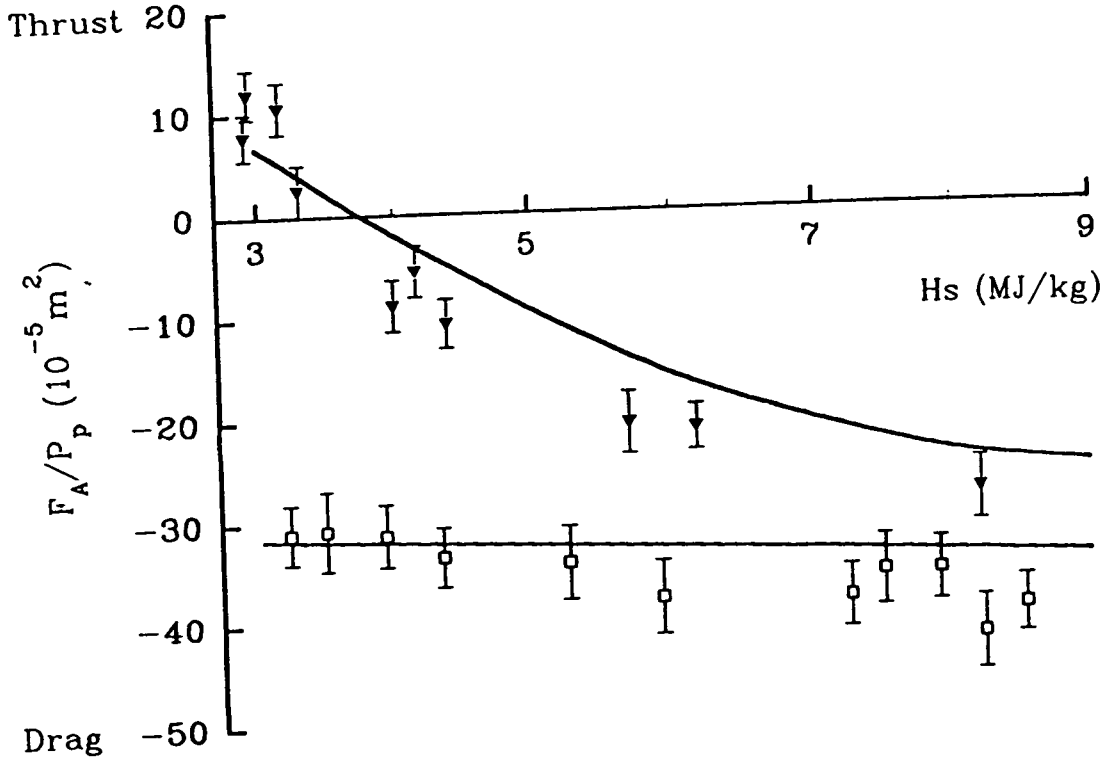

Fig 1